Available online at www.sciencedirect.com
ScienceDirect
Journal of Catalysis 246 (2007) 277–292
JOURNAL OF CATALYSIS
www.elsevier.com/locate/jcat

Characterization and hydrodesulfurization properties of catalysts derived from amorphous metal-boron materials

Greg L. Parks [a], Melissa L. Pease [a], Autumn W. Burns [a], Kathryn A. Layman [a], Mark E. Bussell [a,*], Xianqin Wang [b], Jonathon Hanson [b], José A. Rodriguez [b]

[a] *Department of Chemistry, MS-9150, Western Washington University, Bellingham, WA 98225, USA*
[b] *Department of Chemistry, Brookhaven National Laboratory, Upton, NY 11973, USA*

Received 20 July 2006; revised 5 December 2006; accepted 8 December 2006

Available online 22 January 2007

Abstract

Unsupported and silica-supported amorphous metal-boron materials (Ni-B, Mo-O-B, and Ni-Mo-O-B) were prepared by $NaBH_4$ reduction of aqueous or impregnated metal salts. The resulting materials were characterized by a range of techniques, including conventional and time-resolved X-ray diffraction. The latter technique was used to determine the onset of crystallization of the amorphous materials during annealing in He flow and to identify the phases formed. Annealing of unsupported Ni-B resulted in the crystallization of predominantly Ni_3B, followed by Ni metal, whereas Ni-B/SiO_2 formed Ni and then NiO. There was no evidence for crystallization of B-containing phases for Mo-O-B or Mo-O-B/SiO_2 on annealing; instead, the predominant phase formed was MoO_2. In general, the phases formed for Ni-Mo-O-B and Ni-Mo-O-B/SiO_2 were consistent with those formed in the monometallic materials, but at higher annealing temperatures. Catalysts prepared by sulfiding Ni-B/SiO_2 and Ni-Mo-O-B/SiO_2 materials had significantly higher thiophene HDS activities than conventionally prepared sulfided Ni/SiO_2 and Ni-Mo/SiO_2 catalysts, whereas a sulfided Mo-O-B/SiO_2 catalyst had a dramatically lower HDS activity than a sulfided Mo/SiO_2 catalyst.

1. Introduction

Amorphous metal-boron materials have attracted interest as heterogeneous catalysts since the early work of Brown and co-workers, who found that unsupported Ni-B catalyzed the production of hydrogen from aqueous sodium borohydride ($NaBH_4$) [1,2]. Since then, investigation of the catalytic properties of amorphous metal-boron materials has focused primarily on hydrogenation reactions, although they have been shown to be active for other processes as well, including polymerization and desulfurization [2]. Of particular interest to the current study, Ni-B catalysts have demonstrated greater sulfur tolerance than B-free Ni catalysts. For example, a Ni-B/SiO_2 catalyst was observed to be not only more active and selective for cyclopentadiene hydrogenation than a Ni/SiO_2 catalyst, but also more sulfur tolerant [3]. Based on theoretical calculations, Luo et al. [4] concluded that the S resistance of Ni-B catalysts can be traced to strong interactions between adsorbed S and surface B atoms, preventing the poisoning of active Ni hydrogenation sites.

To the best of our knowledge, there has been only one report in the literature describing the use of amorphous metal-boron materials as catalysts for hydrodesulfurization (HDS). Cheng et al. [5] measured thiophene HDS activities for alumina- and titania-supported Ni-B catalysts. The Ni-B/TiO_2 catalyst was significantly more active than the Ni-B/Al_2O_3 catalyst, which the authors attributed to differences in the thiophene HDS activation energies over the two catalysts [5]. Suslick and coworkers [6] recently reported the results of thiophene HDS measurements for crystalline Co_2B and Ni_3B, both in unsupported form, and found the catalysts to be unstable under HDS conditions and to have relatively low activities. The use of boron as an additive in sulfide-based catalysts has received far greater attention in the literature than the use of amorphous or crystalline boron-containing materials as catalysts [7]. As described by others [8–10], the addition of small amounts of B (<1 wt%) to sulfided Co-Mo/Al_2O_3 and Ni-Mo/Al_2O_3 cat-

* Corresponding author. Fax: +1 360 650 2826.
E-mail address: mark.bussell@wwu.edu (M.E. Bussell).

0021-9517/$ – see front matter
doi:10.1016/j.jcat.2006.12.009

alysts has been observed to increase HDS activity, whereas greater amounts resulted in decreased activity. In each of these cases, the B was added directly to the γ-Al_2O_3 support in the form of boric acid (H_3BO_3) and then calcined before impregnation with metal salts. However, if B was added (as H_3BO_3) after the metals to Co-Mo/Al_2O_3 catalysts only a decrease in HDS activity was observed [11]. The enhanced HDS activity of sulfided Co-Mo/Al_2O_3 and Ni-Mo/Al_2O_3 catalysts to which small amounts of B were added to the support before the metals has been traced to a number of factors, including increased support acidity, improved Co and Mo dispersion, and altered MoS_2 particle morphologies [7,12].

The focus on catalysts derived from amorphous metal-boron materials in the current study stems from our interest in the hydrotreating properties of nonsulfide materials, which has led us to investigate metal carbides, nitrides, and phosphides [13–17]. Oxide-supported molybdenum carbide (β-Mo_2C), nitride (γ-Mo_2N), and phosphide (MoP), for example, have been observed to have higher thiophene HDS activities than oxide-supported sulfided Mo catalysts [13–15,18,19]. Most dramatically, a silica-supported nickel phosphide catalyst (Ni_2P/SiO_2) was observed to be more than 20 times more active than sulfided nickel on the same support (sulf. Ni/SiO_2) [17].

Although we successfully prepared bulk and silica-supported Ni-B materials in the current work, our attempts to prepare bulk and supported Mo-B and Ni-Mo-B materials resulted in only partial reduction of Mo species by aqueous $NaBH_4$. However, the resulting materials were amorphous and, in the case of the Ni-Mo-O-B materials, are novel precursors to highly active thiophene HDS catalysts. In addition to describing the HDS properties of catalysts derived from the amorphous metal-boron materials, we report the detailed characterization of the amorphous-to-crystallization transition of these materials during annealing in flowing He using time-resolved X-ray diffraction (XRD).

2. Experimental

2.1. Catalyst synthesis

2.1.1. Ni-B and Ni-B/SiO_2

An amorphous nickel-boron (Ni-B) catalyst was-prepared by the reduction of nickel acetate ($Ni(C_2H_3O_2)_2{\cdot}4H_2O$, Alfa Aesar, >99% purity) with sodium borohydride ($NaBH_4$, EM Science, 98% purity) using a procedure adapted from that of Glavee et al. [20]. An aqueous solution of 3.01 g of $Ni(C_2H_3O_2)_2{\cdot}4H_2O$ was placed in a 500-ml three-necked flask and then flushed with N_2 (Airgas, 99.999%) and then ~10 L of hydrogen (H_2, Airgas, 99.999%). An aqueous solution of 1.97 g $NaBH_4$ degassed with N_2 was added dropwise with constant mixing. After stirring for 30 min, the solid product was collected by vacuum filtration, then washed three times each with water and then ethanol (C_2H_5OH, Pharmco, 99.5%). While still moist, the product was transferred to a vacuum dessicator and dried under vacuum for 3 h. The dessicator was then back-filled to 1 atm with a 1 mol% O_2/He mixture to passivate the Ni-B product before exposure to the ambient atmosphere.

A silica-supported Ni-B (Ni-B/SiO_2) catalyst with a nominal 30 wt% Ni loading was synthesized using a modified version of the procedure described above for the unsupported Ni-B catalysts. A 5-g sample of silica (SiO_2, Cabot, M-7D, 200 m^2/g), previously calcined at 773 K for 3 h, was impregnated with an aqueous solution of 6.45 g $Ni(C_2H_3O_2)_2{\cdot}4H_2O$ until incipient wetness. Multiple impregnations were needed, and the $Ni(C_2H_3O_2)_2/SiO_2$ precursor was dried at 393 K after each impregnation. A 2-g sample of the $Ni(C_2H_3O_2)_2/SiO_2$ precursor was placed in a 500-ml, three-necked, round-bottomed flask and purged with N_2 followed by H_2 as described above. An aqueous solution of 0.80 g of $NaBH_4$, degassed with N_2, was added dropwise to the $Ni(C_2H_3O_2)_2/SiO_2$ precursor under constant stirring. The $Ni(C_2H_3O_2)_2/SiO_2$ precursor turned black on addition of the $NaBH_4$ solution, accompanied by effervescence and the liberation of heat. The mixture was stirred for 30 min, after which the Ni-B/SiO_2 product was collected by vacuum filtration and washed three times each with nanopure water and then ethanol. The Ni-B/SiO_2 product, kept moist during the washings and filtration, was transferred to a vacuum dessicator, dried, and passivated as described above.

2.1.2. Mo-O-B and Mo-O-B/SiO_2

An amorphous molybdenum catalyst, called Mo-O-B hereinafter, was-prepared by reduction of ammonium heptamolybdate ($(NH_4)_6Mo_7O_{24}{\cdot}4H_2O$, Fisher Scientific, A.C.S. Grade) with $NaBH_4$ by a procedure similar to that described for Ni-B. An aqueous solution of 1.04 g $NaBH_4$ was added dropwise to an aqueous solution of 3.90 g $(NH_4)_6Mo_7O_{24}{\cdot}4H_2O$ under constant stirring. After continued stirring for 30 min, the Mo-B product was filtered under vacuum and washed three times each with water and then ethanol. The Mo-O-B product was dried and passivated as described above.

Synthesis of a silica-supported Mo-O-B (Mo-O-B/SiO_2) catalyst with a nominal Mo loading of 30 wt% was carried out following a procedure similar to that used for the preparation of Ni-B/SiO_2 catalysts, as described above. A 5.00 g sample of SiO_2, calcined at 773 K for 3 h, was impregnated with an aqueous solution of 3.94 g $(NH_4)_6Mo_7O_{24}{\cdot}4H_2O$. Multiple impregnations were necessary, and the $(NH_4)_6Mo_7O_{24}/SiO_2$ catalyst precursor was dried at 393 K after each impregnation.

An aqueous solution of 0.20 g $NaBH_4$ was added dropwise to 2.00 g of the $(NH_4)_6Mo_7O_{24}/SiO_2$ catalyst precursor with constant stirring. After $NaBH_4$ addition, the mixture was stirred for 30 min to ensure that the reaction reached completion. The Mo-B/SiO_2 product was vacuum filtered, washed, dried, and passivated as described above.

2.1.3. Ni-Mo-B and Ni-Mo-B/SiO_2

Amorphous nickel-molybdenum-boron (Ni-Mo-O-B) catalysts with a range of Ni/Mo molar ratios were prepared by reduction of $Ni(NO_3)_2{\cdot}6H_2O$ and $(NH_4)_6Mo_7O_{24}{\cdot}4H_2O$ with $NaBH_4$ following a procedure similar to that described above for Ni-B. The synthesis procedure for a Ni-Mo-O-B catalyst with an expected molar ratio of Ni/Mo = 1.0 is described here. An aqueous solution of 2.00 g $NaBH_4$ was added dropwise to an aqueous solution containing 1.50 g of nickel

nitrate [$Ni(NO_3)_2{\cdot}6H_2O$, Alfa Aesar, 99.999%] and 1.51 g $(NH_4)_6Mo_7O_{24}{\cdot}4H_2O$ under stirring. After continued stirring for 30 min, the Ni-Mo-O-B product was filtered under vacuum, washed three times each with water and then ethanol, then dried and passivated as described above.

Synthesis of a silica-supported Ni-Mo-O-B (Ni-Mo-O-B/SiO_2) catalyst with a theoretical Ni/Mo molar ratio of 0.75 was carried out as follows. A 5.00-g sample of calcined SiO_2 was impregnated with an aqueous solution of 2.44 g $(NH_4)_6Mo_7O_{24}{\cdot}4H_2O$, followed by drying at 393 K. The $(NH_4)_6Mo_7O_{24}/SiO_2$ precursor was then impregnated with an aqueous solution of 2.44 g $Ni(NO_3)_2{\cdot}6H_2O$ with subsequent drying at 393 K. An aqueous solution of 2.01 g $NaBH_4$ was added dropwise to 2.00 g of the $Ni(NO_3)_2$-$(NH_4)_6Mo_7O_{24}/SiO_2$ precursor under stirring. After continued stirring for 30 min, the product was filtered, washed, dried and passivated as described above.

2.1.4. NiO/SiO_2, MoO_3/SiO_2 and $NiO\text{-}MoO_3/SiO_2$

Oxidic precursors of silica-supported, sulfided Ni, Mo, and Ni-Mo catalysts were prepared as described previously [14,16].

2.2. Catalyst characterization

2.2.1. Elemental composition and X-ray photoelectron spectroscopy

The metal (Ni, Mo) and B contents of the unsupported and silica-supported catalysts were determined using inductively coupled plasma–atomic emission spectroscopy (ICP-AES) by Huffman Laboratories, Inc. X-ray photoelectron spectroscopy (XPS) measurements were carried out using a Physical Electronics Quantum 2000 Scanning ESCA Microprobe system with a focused monochromatic Al$K\alpha$ X-ray (1486.7 eV) source and a spherical section analyzer. The XPS spectra were collected at a pass energy of 23.5 or 46.95 eV. The spectra were referenced to an energy scale with binding energies for Cu($2p_{3/2}$) at 932.67 ± 0.05 eV and Au(4f) 84.0 ± 0.05 eV. Binding energies were corrected for sample charging using the C(1s) peak at 284.6 eV for adventitious carbon as a reference. Low-energy electrons and argon ions were used for specimen neutralization.

2.2.2. BET surface area and oxygen chemisorption

Single-point BET surface area and O_2 pulsed chemisorption measurements were obtained using a Micromeritics Pulse-Chemisorb 2700 apparatus. Catalyst samples (∼0.10 g) were placed in a quartz U-tube, degassed in a 60 ml/min flow of He for 30 min at room temperature, followed by a 2 h degassing in a 45 ml/min flow of He at 623 K, then cooled to room temperature under flowing He. The BET measurements were then carried out as described previously [18].

Chemisorption capacity measurements were conducted using a 10.3 mol% O_2/He mixture (Airco) as the probe gas. After treatment in flowing He as described above, samples were sulfided by heating from room temperature to 650 K (5.9 K/min) in a 60-ml/min flow of 3 mol% H_2S/H_2 and holding at 650 K for 2 h. The sulfided samples were then reduced in a 60-ml/min flow of H_2 at 623 K for 1 h, and then degassed in 45 ml/min He at 650 K for 1 h. The chemisorption capacity measurements were carried out at 196 K as described previously [18].

2.2.3. Conventional and time-resolved X-ray diffraction measurements

Conventional X-ray diffraction (XRD) patterns were acquired using a Rigaku GeigerFlex X-ray diffractometer equipped with a copper X-ray source ($\lambda = 1.54178$ Å). XRD patterns were collected for as-prepared catalysts, as well as for catalyst samples annealed to different temperatures in flowing He. For the annealing experiments, approximately 0.1 g of a catalyst was supported on a quartz wool plug placed in a quartz U-tube, where it was purged for 30 min in a 50-ml/min He (Airgas, 99.999%) flow. The sample was then heated to the desired temperature, ranging from 573 to 973 K, in 30 min while continuing the He flow. The annealing temperature was maintained for 30 min, followed by sample cooling to room temperature in the He flow. The sample was passivated with a 50-ml/min flow of a 1 mol% O_2/He flow for 1 h before sample preparation for the XRD measurement.

The time-resolved XRD data were collected at the beamline X7B ($\lambda = 0.922$ Å) of the National Synchrotron Light Source (NSLS) in Brookhaven National Laboratory (BNL) using a MAR345 area detector. The sample was loaded into a sapphire capillary cell attached to a flow system [21–23]. A small resistance heater was wrapped around the capillary, and the temperature was monitored with a 0.1-mm chromel-alumel thermocouple placed in the capillary near the sample. Under a helium flow of ∼20 ml/min, the sample was heated from 298 to 1073 K within 2 h, then cooled to 298 K over 1 h. Diffraction patterns were collected during the heating and cooling processes. The data analysis consisted of several steps. The original powder rings were first integrated with the FIT2D code [24]; the FIT2D parameters for the integration of the data were obtained from LaB_6 powder patterns. The time-resolved XRD pattern files were finally plotted using IDL software [25].

2.2.4. Infrared spectroscopy of adsorbed CO

The IR spectroscopic experiments were conducted in an ion-pumped (110 L/s) ultra-high-vacuum (UHV) chamber with a base pressure of $\sim 5 \times 10^{-9}$ Torr, equipped with a Mattson RS-1 FTIR spectrometer outfitted with a narrow-band MCT detector interfaced to a personal computer for data acquisition and treatment. The chamber also contains a high-pressure cell that can be isolated from the UHV chamber. This system has been described in detail previously [26].

Approximately 7 mg of the desired catalyst was pressed at 10,000 psi into a nickel metal mesh (50 × 50 mesh size, 0.002 in. wire diameter); the area of the pressed samples was 0.80 cm^2. A chromel-alumel thermocouple was spot-welded to the nickel mesh to monitor the temperature of the sample. This assembly was then mounted onto a sample holder equipped with resistive heating and liquid nitrogen cooling. After mounting in the UHV system, the catalyst samples were evacuated to 10^{-3} Torr over a period of ∼30 min. Unless otherwise stated, the catalysts were then either reduced or sulfided in situ. Specif-

ically, the catalysts were reduced in flowing H_2 (60 sccm) at 475 K for 1 h or sulfided in 100 Torr of a 3 mol% H_2S/H_2 mixture at 650 K for 15 min. To remove weakly adsorbed species from the surface of the reduced and sulfided catalysts, the high-pressure cell was then evacuated to $\sim 1 \times 10^{-7}$ Torr before the sample was annealed at 475 K (reduction) or 650 K (sulfidation) for 1 min. After pretreatment, the reduced/sulfided sample was cooled to room temperature at a pressure of $\sim 1 \times 10^{-8}$ Torr, and a background IR spectrum was acquired. An IR spectrum of adsorbed CO was then collected at 298 K while the catalyst sample was in the presence of 5.0 Torr CO.

Transmission FTIR spectra were acquired in the 4000–1000 cm^{-1} range by collecting 128 scans at 4-cm^{-1} resolution. The sample spectrum was ratioed against a background spectrum acquired using a blank nickel mesh mounted in the sample holder and a pressure of 5.0 Torr CO. All IR spectra were prepared by subtracting the IR spectrum obtained before dosing from the IR spectrum acquired after dosing. The IR spectra presented in this study have been reproduced without any smoothing treatment.

2.3. Thiophene HDS activity measurements

Thiophene HDS activity measurements were carried out using an atmospheric pressure flow reactor outfitted with a gas chromatograph (HP 5890 Series II). The gas chromatograph was equipped with a flame ionization detector for on-line analysis of thiophene and hydrocarbon products. The flow reactor system and the specifics of the HDS activity measurements have been described in detail previously [18].

Before measurement of thiophene HDS activities, the silica-supported Ni-B, Mo-O-B, and Ni-Mo-O-B catalysts were subjected to one of two different pretreatments: (1) reduction in H_2 by heating the catalyst sample from room temperature to 650 K (5.9 K/min) in a 60-ml/min flow of H_2 and holding at 650 K for 2 h, or (2) sulfidation by heating from room temperature to 650 K (5.9 K/min) in a 60 ml/min flow of 3 mol% H_2S/H_2 and holding at 650 K for 2 h. The oxidic precursors of the silica-supported Ni, Mo, and Ni-Mo catalysts were subjected only to the sulfidation procedure. After catalyst pretreatment, the temperature was adjusted to the reaction temperature of 643 K, and the flow was switched to a 3.2 mol% thiophene/H_2 reactor feed (50 ml/min). The reaction was carried out for 24 h, with automated sampling of the gas effluent done at 1-h intervals. Thiophene HDS activities (nmol Th/g cat s) were calculated from the total product peak areas taken from the chromatogram after 24 h.

3. Results

3.1. Catalyst characterization

The metal (Ni, Mo) and B contents of the unsupported and silica-supported amorphous materials prepared in this study (as well as surface compositions in some cases), along with the BET surface areas and O_2 chemisorption capacities of the supported materials, are listed in Table 1. The monometallic Ni materials have significant B content and hereinafter are referred to as Ni-B for the bulk phase and Ni-B/SiO_2 for the supported phase. The composition determined for unsupported Ni-B ($Ni_{1.95}B_{1.00}$) is similar to that reported by others, indicating that Ni:B molar ratios near 2:1 are typical [2,27]. Recently, however, compositions ranging from $Ni_{1.33}B_{1.00}$ [28] to $Ni_{3.10}B_{1.00}$ [29] have been reported. The Ni-B/SiO_2 catalyst is more B-rich than the unsupported Ni-B, but some of the B likely is associated with the silica support. Others have reported compositions for silica-supported Ni-B materials ranging from $Ni_{1.57}B_{1.00}$ [30] to $Ni_{3.35}B_{1.00}$ [31].

The monometallic Mo materials have low B content and, as described later, significant O content; consequently, hereinafter these materials are referred to as Mo-O-B for the bulk phase and Mo-O-B/SiO_2 for the supported phase. Similarly, the bimetallic Ni-Mo materials contain significant amounts of O (in addition to B) and are referred to as Ni-Mo-O-B for the bulk phase and Ni-Mo-O-B/SiO_2 for the supported material. A search of the literature revealed two reports describing the synthesis of amorphous Ni-Mo materials by borohydride reduction, with an aqueous mixture of nickel chloride and sodium molybdate used in both cases [32,33]. The only characterization information reported was that the majority of the Mo in the amorphous Ni-Mo material from the most recent study was in the +3 oxidation state as determined by XPS [33].

Table 1
Properties of unsupported and silica-supported Ni-B, Mo-O-B, and Ni-Mo-O-B catalysts

Catalyst	Bulk composition	Surface composition	BET surface area (m^2/g)	O_2 chemisorption (μmol O_2/g)
Ni-B	$Ni_{1.95}B_{1.00}$	$Ni_{1.6}B_{1.0}$	–	–
Mo-O-B	$Mo_{16.6}B_{1.00}$	$Mo_{12.6}B_{1.0}$	–	–
Ni-Mo-O-B (Ni/Mo = 1.0)	$Ni_{1.10}Mo_{1.11}B_{1.00}$	$Ni_{1.1}Mo_{1.9}B_{1.0}$	–	–
Mo-O-B/SiO_2	$Mo_{9.81}B_{1.00}$	$Mo_{8.9}B_{1.0}$	72	22
Ni-Mo-O-B/SiO_2 (Ni/Mo = 0.12)	$Ni_{0.43}Mo_{3.59}B_{1.00}$	–	75	10
Ni-Mo-O-B/SiO_2 (Ni/Mo = 0.26)	$Ni_{0.78}Mo_{3.03}B_{1.00}$	–	84	18
Ni-Mo-O-B/SiO_2 (Ni/Mo = 0.33)	$Ni_{1.13}Mo_{3.38}B_{1.00}$	–	88	13
Ni-Mo-O-B/SiO_2 (Ni/Mo = 0.45)	$Ni_{1.44}Mo_{3.22}B_{1.00}$	–	82	17
Ni-Mo-O-B/SiO_2 (Ni/Mo = 0.99)	$Ni_{1.93}Mo_{1.95}B_{1.00}$	$Ni_{2.9}Mo_{3.4}B_{1.00}$	92	26
Ni-Mo-O-B/SiO_2 (Ni/Mo = 2.22)	$Ni_{1.32}Mo_{0.59}B_{1.00}$	–	93	93
Ni-Mo-O-B/SiO_2 (Ni/Mo = 5.52)	$Ni_{1.71}Mo_{0.31}B_{1.00}$	–	120	195
Ni-B/SiO_2	$Ni_{1.65}B_{1.00}$	$Ni_{2.8}B_{1.0}$	109	251

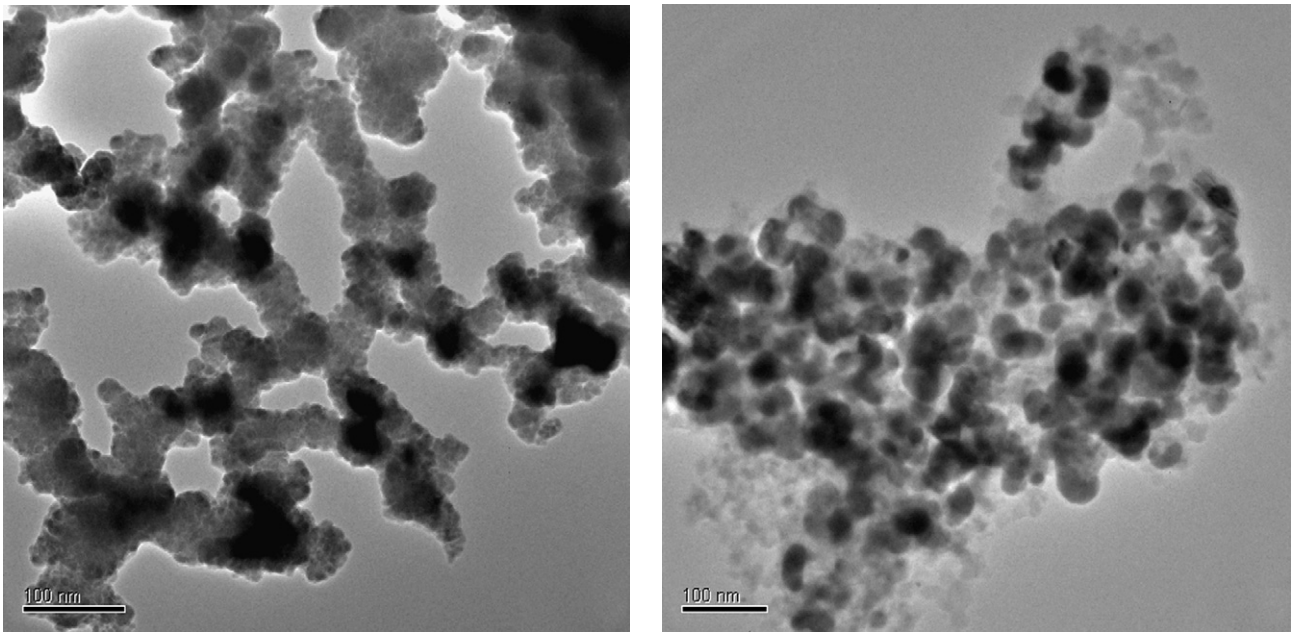

(a) (b)

Fig. 1. TEM images of (a) unsupported and (b) silica-supported Ni-B catalysts in as-prepared form.

A TEM image of unsupported Ni-B (Fig. 1a) reveals that the sample comprises aggregates of spherical-shaped, amorphous particles of ∼5 nm in diameter, as confirmed by higher-resolution images (not shown). These observations are consistent with the results recently reported by Li et al. [27] and Fang et al. [29], who observed spherical amorphous Ni-B particles but with larger diameters (∼10 and ∼35 nm, respectively). TEM images of unsupported Ni-B annealed to 773 K in flowing He indicate that the small Ni-B particles have sintered to give much larger, crystalline particles, which is consistent with the XRD pattern of a Ni-B sample annealed to 773 K (see Fig. 5a). Interestingly, the TEM image of the Ni-B/SiO_2 catalyst (21.6 wt% Ni) shown in Fig. 1b shows relatively large Ni-B particles with diameters of 20–40 nm. This range of Ni-B particle sizes for the Ni-B/SiO_2 catalyst is similar to the observations of Chen et al. [28] for a Ni-B/MCM-41 catalyst (no loading given), in which Ni-B particle sizes of 20–60 nm were observed, but different from those for a Ni-B/SBA-15 catalyst (9.84 wt% Ni) with more uniformly sized Ni-B particles ∼6.5 nm in diameter. TEM images of the Ni-B/SiO_2 catalyst annealed to 773 K in He revealed no substantial changes in the supported Ni-B particles other than crystallization.

TEM images of unsupported Mo-O-B and Mo-O-B/SiO_2 (19.2 wt% Mo) are shown in Fig. 2. The amorphous Mo-O-B particles are quite large in both materials, with particle diameters of 80–100 nm for Mo-O-B and 60–80 nm for Mo-O-B/SiO_2. Fig. 3 shows TEM images for unsupported and silica-supported Ni-Mo-O-B. The unsupported Ni-Mo-B material has particle sizes of 90–100 nm, similar to the unsupported Mo-O-B sample. For the Ni-Mo-O-B/SiO_2 catalyst (7.5 wt%, Ni, 12.3 wt% Mo, Ni/Mo = 0.99), the Ni-Mo-O-B particle size is ∼80 nm. Using TEM, Fang et al. [29] observed unsupported Ni-Cr-B with a composition $Ni_{3.57}Cr_{0.17}B_{1.00}$ to have particle sizes of ∼7 nm, substantially smaller than the ∼35 nm particles of unsupported Ni-B. Not surprisingly, the Ni-Cr-B material had a surface area four times higher than that of the unsupported Ni-B. The Cr was determined to have a +3 oxidation state, which the authors assigned to the partial reduction of aqueous CrO_4^{2-} to Cr_2O_3 on addition of KBH_4 [29].

XPS spectra for the silica-supported Ni-B, Mo-O-B, and Ni-Mo-O-B (Ni/Mo = 0.99) catalysts are shown in Fig. 4. Because the catalysts were passivated in a 1 mol% O_2/He mixture after synthesis, peaks for oxidized metal and B species dominate the XPS spectra. For the Ni-B/SiO_2 catalyst, two peaks are apparent in the Ni($2p_{3/2}$) region at 851.5 and 855.2 eV. The high-binding energy species is assigned to Ni^{2+} species in the passivation layer surrounding the Ni-B particles and likely is in the form of $Ni(OH)_2$, for which Ni($2p_{3/2}$) binding energies of 855.6–856.6 eV have been reported [34]. The low-binding energy Ni species is assigned to Ni bonded directly to B; its binding energy of 851.5 eV is below that of nickel metal (Ni^0, 852.5–852.9 eV [35]) as well as the Ni($2p_{3/2}$) binding energies of 852.2–853.0 eV reported by others for Ni-B in unsupported and supported forms [31,36–38]. It has been suggested that B donates electron density to Ni in Ni-B [3,36]. The only peak observed in the B(1s) region is located at 191.1 eV, which lies between the binding energies of elemental B (187.3 eV [39]) and B in B_2O_3 (192.9 eV [39]). The B(1s) binding energy measured for the Ni-B/SiO_2 catalyst lies between the values reported by others for unsupported Ni-B catalysts (188.2–188.4 eV) [28] and Ni-B/Al_2O_3 catalysts (192.1–192.2 eV) [38]; two peaks were observed in each case. The peak at 188.2–188.4 was assigned to B bonded to Ni; based on the binding energy, the authors concluded that B donates electron density to Ni, in agreement with earlier work by Okamoto et al. [36,40]. The peak at 192.1–192.2 eV was assigned to oxidized B species, presumably at the surface of the Ni-B particles.

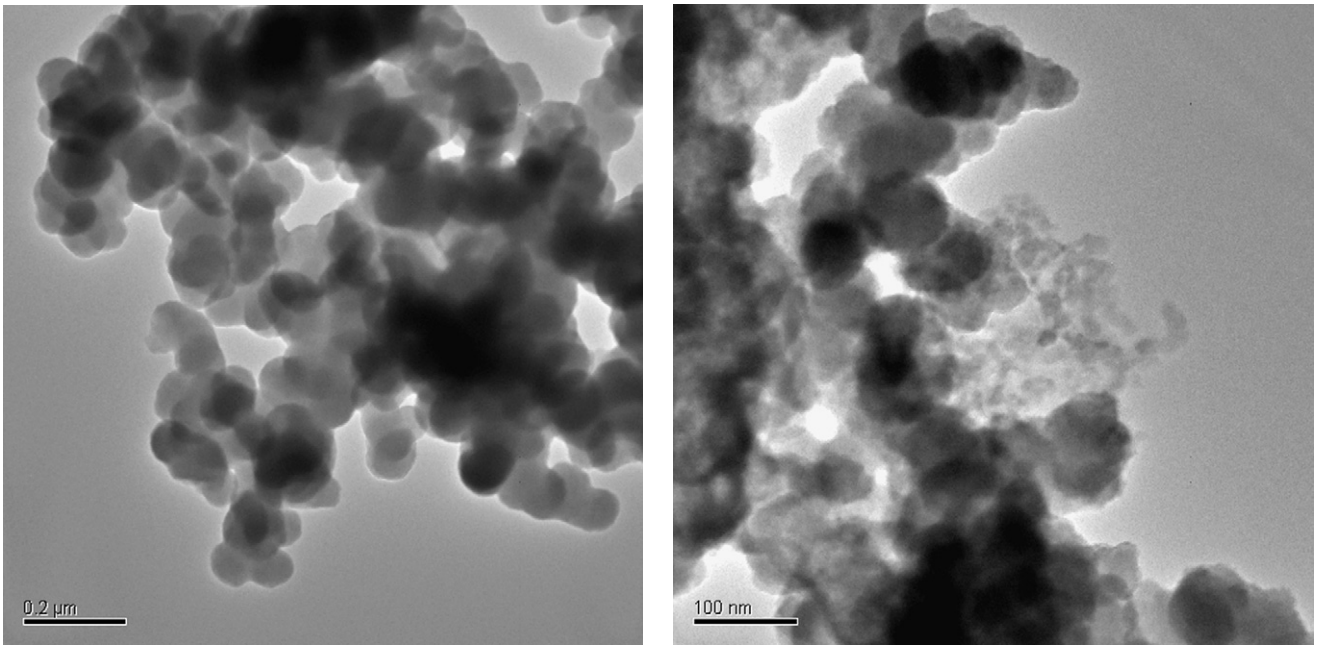

(a) (b)

Fig. 2. TEM images of (a) unsupported and (b) silica-supported Mo-O-B catalysts in as-prepared form.

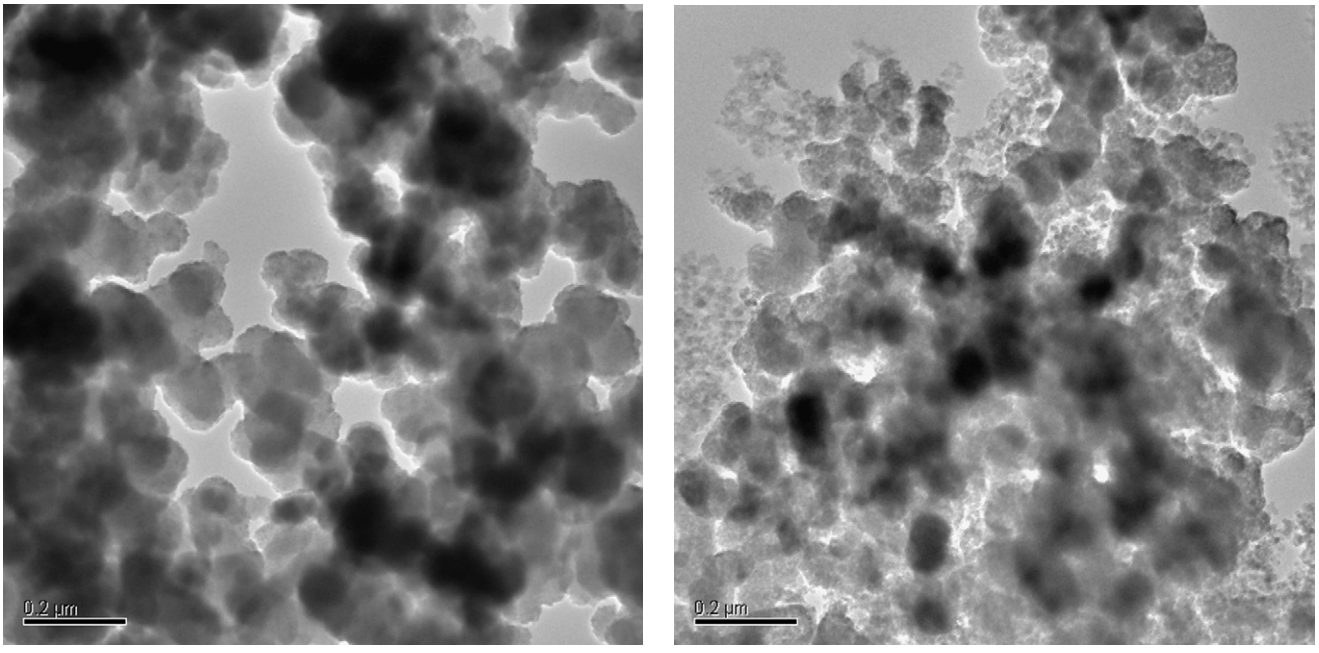

(a) (b)

Fig. 3. TEM images of (a) unsupported and (b) silica-supported Ni-Mo-O-B catalysts in as-prepared form.

The XPS spectrum of the Mo-O-B/SiO_2 catalyst indicates that only partial reduction of the Mo^{6+} ions occurred during treatment of the dried $(NH_4)_6Mo_7O_{24}/SiO_2$ precursor with aqueous $NaBH_4$. Two peaks, at 229.8 and 231.3 eV, are apparent in the Mo($3d_{5/2}$) region for the Mo-O-B/SiO_2 catalyst. The former peak has a binding energy consistent with Mo^{4+} in MoO_2 (229.1–230.9 eV [39]); the latter peak's binding energy is similar to that of Mo^{5+} in Mo_2O_5, (231.7 eV [41]). The binding energies of the Mo species in Mo-O-B/SiO_2 are at higher values than for Mo metal (227.6–228.1 eV [39]), and Mo in Mo_2B_5 (227.9 eV [39]) and MoB_2 (227.3 eV [39]). The B(1s) binding energy of 191.2 eV is substantially higher than that of B in Mo_2B_5 (187.7 eV [39]) and MoB_2 (188.4 eV [39]) and is indicative of oxidized B species, as was observed for the Ni-B/SiO_2 catalyst.

The XPS spectrum of the Ni-Mo-O-B/SiO_2 catalyst is essentially a composite of those of the silica-supported Ni-B and Mo-O-B catalysts, except that the peaks associated with the most reduced Ni and Mo species are of lower intensity. Thus, although the same Ni, Mo, and B species are present in the Ni-

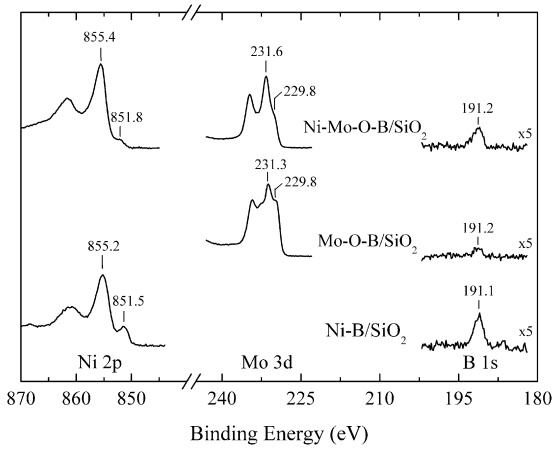

Fig. 4. XPS spectra of silica-supported Ni-B, Mo-O-B, and Ni-Mo-O-B catalysts in as-prepared form.

Mo-O-B/SiO_2 catalyst, the oxidized surface layer covering the particles is apparently thicker.

A number of techniques, including XRD and differential scanning calorimetry (DSC), have been used by others to characterize amorphous-to-crystalline transitions for unsupported and silica-supported Ni-B catalysts. XRD has been used to identify the crystalline phases formed on annealing. In the current study, we combined conventional and time-resolved XRD to carefully pinpoint the amorphous-to-crystalline transitions for the different materials and also to identify the temperature regimes in which the various phases formed are stable in a flowing He atmosphere. Fig. 5a shows XRD patterns for as-prepared Ni-B and a Ni-B sample annealed at 773 K, as well as a reference pattern for Ni_3B (card no. 73-1792 [42]). The XRD pattern for the as-prepared Ni-B exhibits a single broad peak at ∼45.0° that is characteristic of amorphous Ni-B alloys [27–29,43]. The XRD pattern of a Ni-B sample annealed to 773 K in flowing He is in good agreement with the reference pattern of Ni_3B. Depending on the synthesis and annealing conditions, single phases or combinations of Ni_3B, Ni_2B, or Ni metal are typically observed [2,27,28,33,43]. The overlap of the XRD patterns for Ni_3B and Ni_2B makes it difficult to determine whether Ni_2B is present in our Ni-B sample annealed to 773 K, but we can conclude that if it is present at all, its concentration is quite low. Examining the sequence of time-resolved XRD patterns in Fig. 5b allows us to determine the temperature of crystallization of amorphous Ni-B to give Ni_3B, as well as the subsequent decomposition of Ni_3B to give crystalline Ni metal. Noting that the X-ray wavelength is 0.9220 Å for the time-resolved experiments, the broad peak characteristic of amorphous Ni-B is located at ∼28° in the first XRD pattern, which corresponds to the as-prepared material at 298 K. During heating in flowing He, the XRD patterns remain unchanged up to 633 K, at which point peaks associated with crystalline Ni_3B first appear. With continued heating, the Ni_3B XRD peaks strengthen in intensity, reaching a maximum at ∼723 K, and then disappear by ∼933 K. Although difficult to distinguish from Ni_3B peaks,

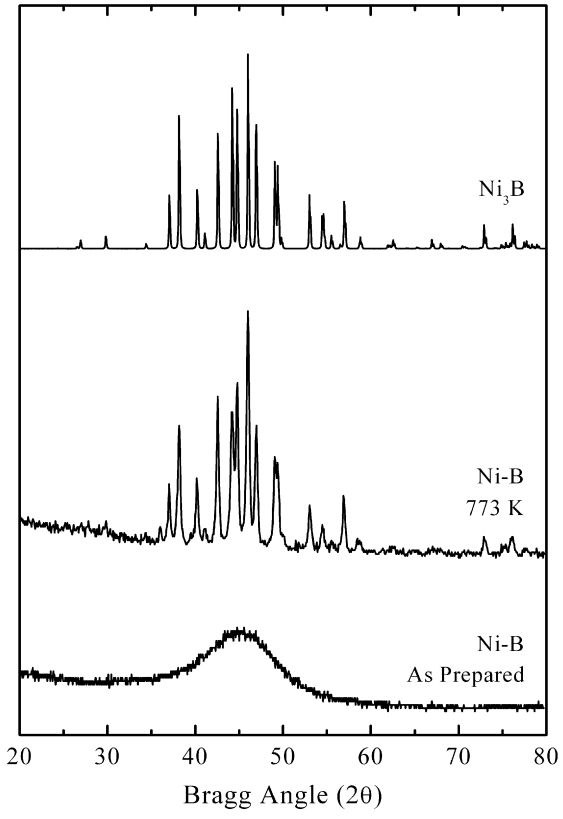

(a)

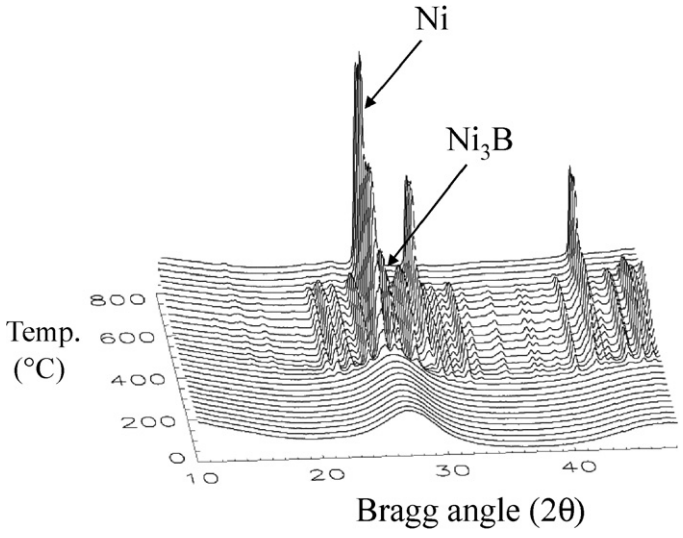

(b)

Fig. 5. (a) Conventional XRD patterns (λ = 1.54178 Å) of an as-prepared unsupported Ni-B catalyst, a Ni-B catalyst annealed to 773 K in flowing He, and a reference pattern for Ni_3B. (b) Time-resolved XRD patterns (λ = 0.9220 Å) acquired while heating (6.5 K/min) as-prepared unsupported Ni-B catalyst in flowing He.

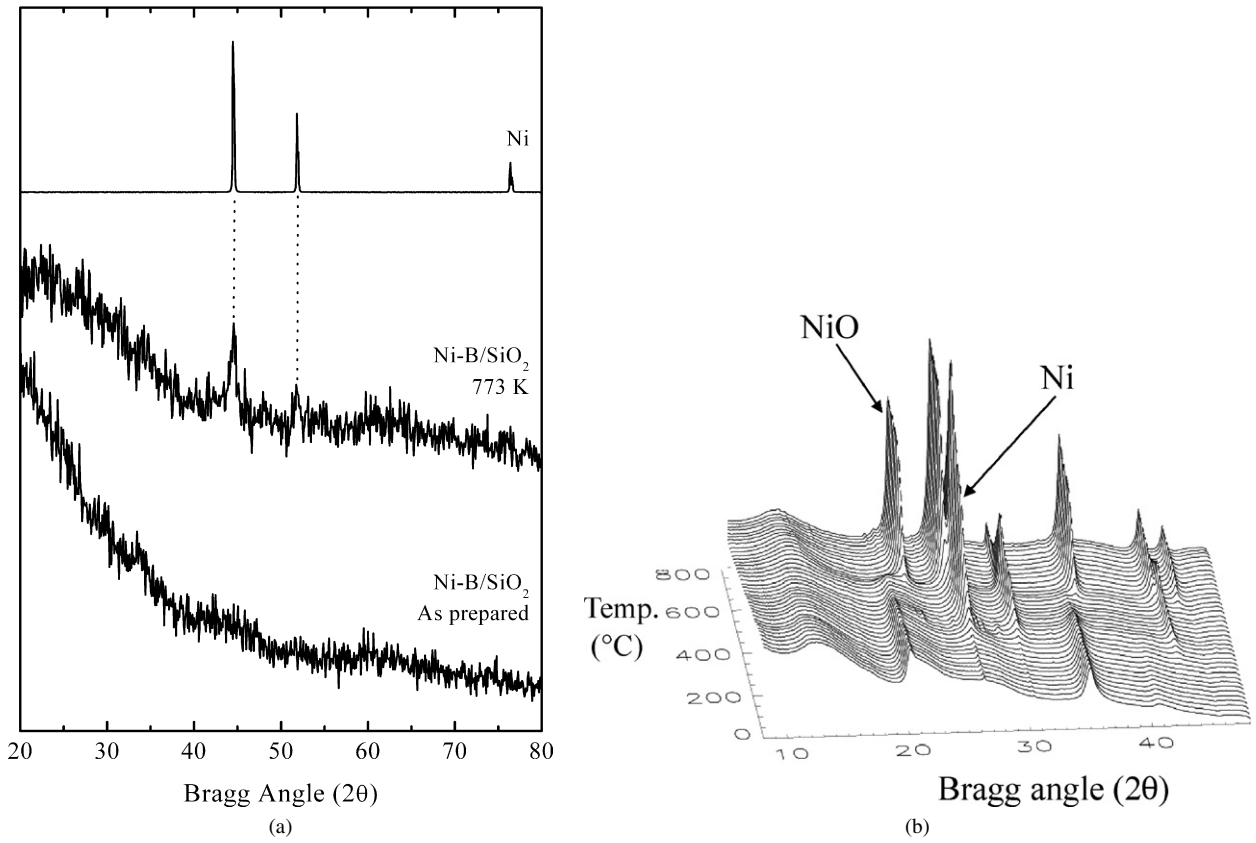

Fig. 6. (a) Conventional XRD patterns ($\lambda = 1.54178$ Å) of an as-prepared Ni-B/SiO_2 catalyst, a Ni-B/SiO_2 catalyst annealed to 773 K in flowing He, and a reference pattern for Ni metal. (b) Time-resolved XRD patterns ($\lambda = 0.9220$ Å) acquired while heating (6.5 K/min) an as-prepared Ni-B/SiO_2 catalyst in flowing He.

new peaks (e.g., 30.3°) begin to appear at ∼713 K that are assigned to the XRD pattern of Ni metal. The Ni metal peaks grow steadily in intensity before temporarily reaching a plateau at ∼873 K, then significantly increasing in intensity starting at ∼933 K. The growth of the Ni metal XRD peaks above ∼933 K corresponds with the decomposition of Ni_3B, as determined by the loss of intensity of Ni_3B XRD peaks. Once the Ni_3B has completely decomposed at ∼933 K, the intensity of the Ni metal XRD peaks stabilizes.

For silica-supported Ni-B, the XRD pattern for the as-prepared catalyst (Fig. 6a), shows an increasing background at decreasing Bragg angles associated with the amorphous silica support, as well as a broad low-intensity peak at ∼43° assigned to the supported amorphous Ni-B particles. The XRD pattern of a sample of the Ni-B/SiO_2 catalyst annealed to 773 K in flowing He shows relatively low-intensity peaks that can be readily assigned to Ni metal, with no indication of a crystalline B-containing phase. This observation is consistent with those of others for Ni-B/SiO_2, Ni-B/C, and Ni-B/Al_2O_3 catalysts annealed to >600 K [33,38,44]. The first XRD pattern in Fig. 6b, which corresponds to as-prepared Ni-B/SiO_2 at 298 K, shows two broad peaks at 20° and 35° that do not appear at the corresponding 2θ values in the conventional XRD pattern of the same catalyst (see Fig. 6a) and cannot be attributed to any expected phase(s). The sequence of time-resolved XRD patterns for the Ni-B/SiO_2 catalyst shows the crystallization of silica-supported Ni-B to give Ni metal beginning at ∼533 K, as indicated by the growth of an XRD peak at 26.0°. This and other Ni metal XRD peaks reach a maximum in intensity at ∼813 K, above which the intensity begins to decrease. Above ∼813 K, the Ni metal undergoes a reaction with surface O to form NiO (card no. 06-595 [42]), as indicated by the growth of XRD peaks associated with NiO (e.g., 21.8°) at the expense of Ni peaks.

As described above, the amorphous materials produced by $NaBH_4$ reduction of aqueous and silica-supported $(NH_4)_6Mo_7O_{24}$ have low B content. XRD patterns for the annealed materials are consistent with these observations. Shown in Fig. 7a are XRD patterns for as-prepared unsupported Mo-O-B and a sample of this material annealed to 773 K in flowing He, along with some reference patterns. The XRD pattern for the as-prepared sample shows a single broad peak at ∼27.5°, indicating that the material is amorphous, whereas the pattern for the sample annealed to 773 K in flowing He shows peaks characteristic of one or more crystalline phases. The most intense peaks in the pattern for the annealed Mo-O-B sample correspond to MoO_2 (card no. 32-0671 [42]), whereas less-intense peaks can be assigned to minor phases of MoO_3 (card no. 35-0609 [42]) and possibly MoB (card no. 06-0644 [42]). If all of the B in the Mo-O-B sample were present in the form of MoB, then this boride phase would constitute approximately 8 mol% of the sample. As a result, it is not surprising that the peaks at 30.3° and 42.4° are of very weak intensity. The sequence of time-resolved XRD patterns shown in Fig. 7b indicates that

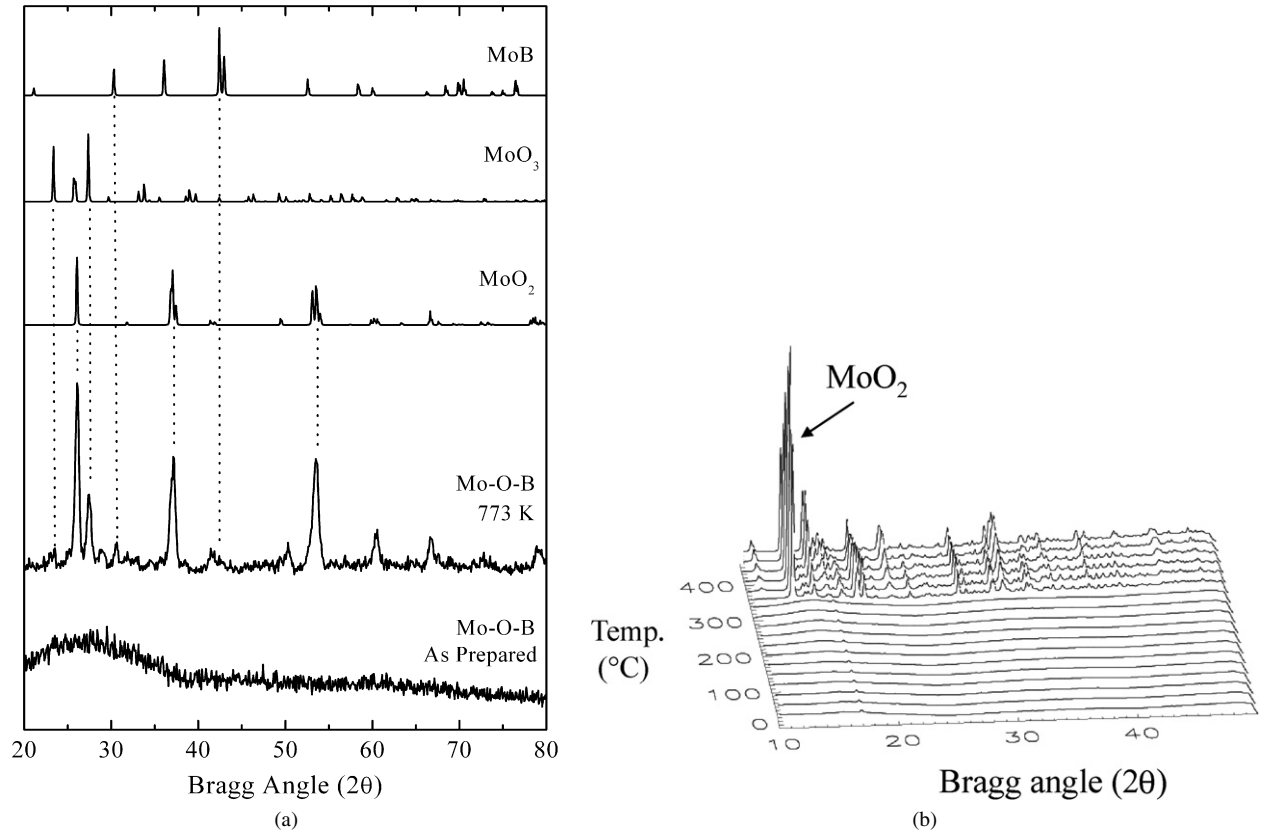

Fig. 7. (a) Conventional XRD patterns ($\lambda = 1.54178$ Å) of an as-prepared unsupported Mo-O-B catalyst, a Mo-O-B catalyst annealed to 773 K in flowing He, and reference patterns for MoO_2, MoO_3, and MoB. (b) Time-resolved XRD patterns ($\lambda = 0.9220$ Å) acquired while heating (6.5 K/min) as-prepared unsupported Mo-O-B catalyst in flowing He.

the unsupported Mo-O-B remains amorphous until ∼613 K, at which point the sample rapidly crystallizes to give primarily MoO_2 and some MoO_3, as indicated by the growth of strong and weak peaks at 15.5° and 16.4°, respectively. There is no evidence in the sequence of XRD patterns indicating formation of a crystalline B-containing phase. Due to experimental problems, it was not possible to continue the time-resolved XRD measurements above ∼733 K for the unsupported Mo-O-B sample.

The XRD results for the Mo-O-B/SiO_2 catalyst are consistent with those of the unsupported Mo-O-B sample. XRD patterns for as-prepared and annealed (773 K) samples of a Mo-O-B/SiO_2 catalyst, along with reference patterns for MoO_2 and MoO_3, are shown in Fig. 8. The XRD pattern for the as-prepared sample shows only an increasing background, indicating that the material is amorphous, whereas the pattern for the sample annealed to 773 K shows peaks characteristic of MoO_2 and MoO_3. As for the unsupported Mo-O-B, crystallization of the amorphous silica-supported Mo-O-B occurs rapidly, starting at a temperature of ∼623 K, to give almost exclusively MoO_2 with a minor amount of MoO_3. After their rapid increase in size, the peaks associated with MoO_2 increase gradually with increased temperature, whereas the peaks associated with MoO_3 decrease in intensity and disappear by 873 K.

XRD patterns for as-prepared and annealed (873 K) Ni-Mo-O-B and Ni-Mo-O-B/SiO_2 materials are shown in Figs. 9 and 10, respectively. The XRD patterns for the as-prepared samples are indicative of amorphous materials, whereas patterns for annealed samples exhibit XRD peaks associated with Ni metal and MoO_2, as well as possibly MoB in the silica-supported material. XRD peaks assigned to Ni and MoO_2 are narrow and intense for the unsupported Ni-Mo-O-B sample annealed to 873 K, as is the MoO_2 reflection at 26° for the annealed Ni-Mo-O-B/SiO_2 catalyst, but the most prominent Ni peak at 44.6° is barely discernible above the background for the silica-supported material.

The time-resolved XRD measurements for the Ni-Mo-O-B and Ni-Mo-O-B/SiO_2 materials show distinct differences from those of the unsupported and silica-supported Ni-B and Mo-O-B materials. For the unsupported Ni-Mo-B, the onset of crystallization of Ni and MoO_2 is observed at ∼550 and ∼795 K, respectively; no formation of Ni_3B or MoO_3 is observed. The formation of crystalline Ni in Ni-Mo-O-B occurs at a substantially lower temperature than for Ni-B, for which crystalline Ni formation starts at ∼713 K when crystalline Ni_3B (formed at 633 K) begins to decompose. On the other hand, the onset of crystallization of MoO_2 is shifted from ∼613 K for Mo-O-B to ∼795 K for Ni-Mo-O-B. For the silica-supported materials, the onset of crystallization is seen at ∼675 K for Ni and ∼790 K for MoO_2. These crystallization temperatures are shifted substantially higher than for Ni-B/SiO_2 and Mo-O-B/SiO_2, for which Ni and MoO_2 crystallization start at 523 and 633 K, respectively.

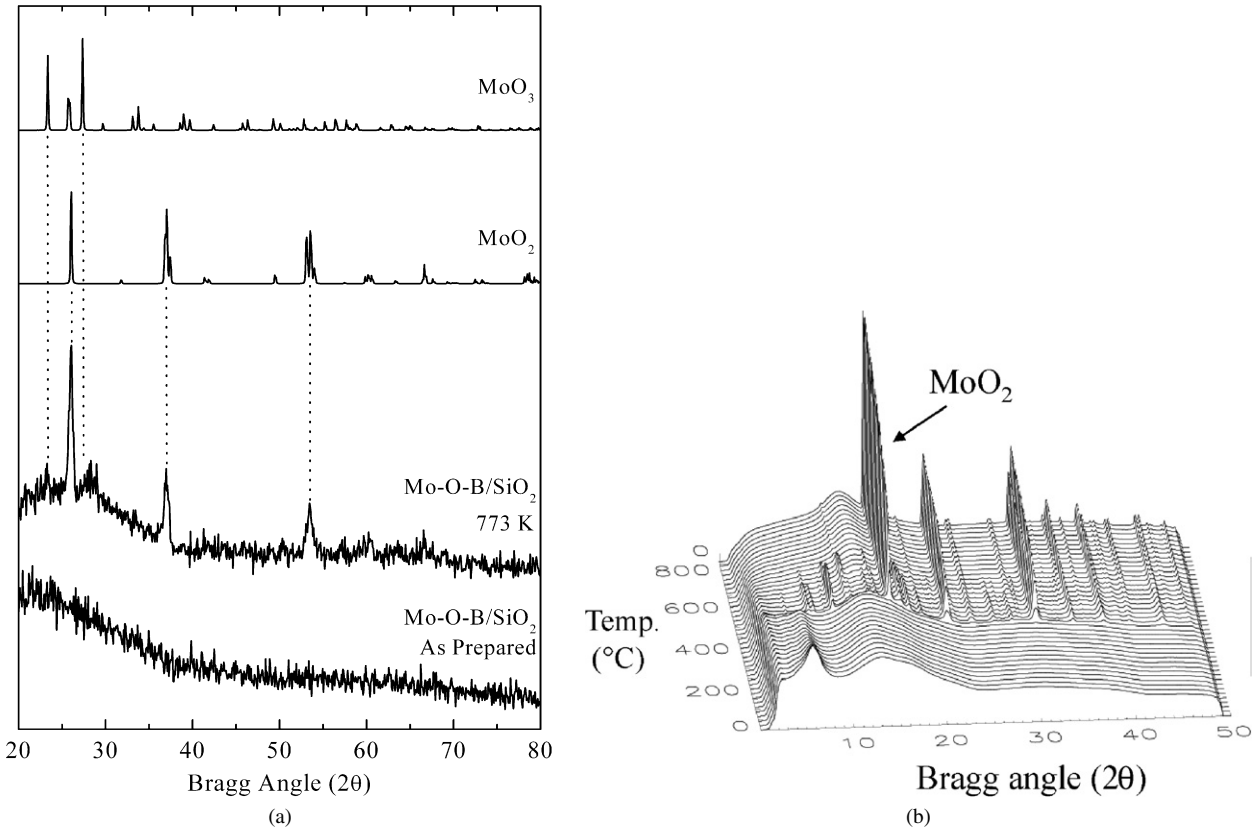

Fig. 8. (a) Conventional XRD patterns ($\lambda = 1.54178$ Å) of an as-prepared Mo-O-B/SiO_2 catalyst, a Mo-O-B/SiO_2 catalyst annealed to 773 K in flowing He, and a reference pattern for MoO_2. (b) Time-resolved XRD patterns ($\lambda = 0.9220$ Å) acquired while heating (6.5 K/min) an as-prepared Mo-O-B/SiO_2 catalyst in flowing He.

Infrared spectroscopy of adsorbed CO on reduced and sulfided Ni-Mo-O-B/SiO_2 and Ni-Mo/SiO_2 catalysts at room temperature are shown in Fig. 11. The IR spectra for the reduced catalysts (Fig. 11a), which were treated in flowing H_2 at 475 K, reveal significant differences. The IR spectrum for the reduced Ni-Mo/SiO_2 catalyst shows ν_{CO} absorbances at 2048, 2141, and 2189 cm^{-1} that can be assigned to CO adsorbed on Ni^0, Ni^+, and Mo^{4+} sites, respectively, with the CO bonded linearly in each case [45–50]. The peak centered at 2048 cm^{-1} is quite broad, most likely because it comprises overlapping absorbance features corresponding to CO adsorbed on various Ni^0 sites, as well as possibly on Ni-promoted $Mo^{\delta+}$ sites. The observation of CO adsorbed on oxidized Ni and Mo sites is not surprising given the mild reducing conditions used. The IR spectrum of adsorbed CO on a reduced Ni-Mo-O-B/SiO_2 catalyst shows dramatic differences, with ν_{CO} absorbance features at ∼1903, 1953, 2006, 2040, 2059, 2127, and 2187 cm^{-1}. Consistent with the reduced Ni-Mo/SiO_2 catalyst, the peaks at 2127 and 2187 cm^{-1} are assigned to CO adsorbed to Ni^+ and Mo^{4+} sites, respectively. The envelope of absorbance features in the 1975–2075 cm^{-1} region is much more intense than the broad peak centered at 2048 cm^{-1} in the IR spectrum of the reduced Ni-Mo/SiO_2 catalyst, indicating that there are substantially more sites at the surface of the reduced Ni-Mo-O-B/SiO_2 catalyst. The ν_{CO} absorbances at ∼1903 and 1953 cm^{-1} are assigned to bridge-bonded CO on Ni^0 sites, and the peak at 2040 cm^{-1} is assigned to linearly bonded CO on Ni^0 sites [45,46]. The peak at 2059 cm^{-1} is tentatively assigned to multiply coordinated CO molecules adsorbed on highly defected Ni^0 sites [46], although absorbance due to adsorbed nickel tetracarbonyl species or CO adsorbed to Ni-promoted $Mo^{\delta+}$ sites also would be expected in this region. Assigning the peak at 2006 cm^{-1} is more difficult, because this peak is located at a wavenumber somewhere between the ranges assigned to bridge-bonded (1800–1980 cm^{-1}) and linearly bonded (2040–2070 cm^{-1}) CO on Ni^0 sites and at a different wavenumber than the ν_{CO} absorbances observed for adsorbed CO on a reduced Ni-Mo/SiO_2 catalyst (see above) or on a mildly reduced Ni-Mo/Al_2O_3 catalyst (1950, 2065, and 2170 cm^{-1}) [50]. Instead, based on the assignments of others for peaks in the 1997–2025 cm^{-1} range for adsorbed CO on reduced Mo/Al_2O_3 catalysts [47,51], the peak at 2006 cm^{-1} is tentatively assigned to CO adsorbed to Mo^0 sites.

In contrast to the IR spectral results for the reduced catalysts, the IR spectra of adsorbed CO on the sulfided Ni-Mo/SiO_2 and Ni-Mo-O-B/SiO_2 catalysts shown in Fig. 11b indicate that the adsorption sites exposed on these catalysts are quite similar. For the sulfided Ni-Mo/SiO_2 catalyst, ν_{CO} absorbances are observed at 2095 and ∼2112 cm^{-1}; these are assigned to Ni-promoted $Mo^{\delta+}$ and unpromoted Mo^{2+} sites, respectively [52–55]. The IR spectrum of adsorbed CO on the Ni-Mo-O-B/SiO_2 catalyst exhibits ν_{CO} absorbance features at ∼1970, 2040, 2088, and 2144 cm^{-1}, respectively. The peaks at ∼1970 and 2040 cm^{-1} are assigned to bridge-bonded and linearly

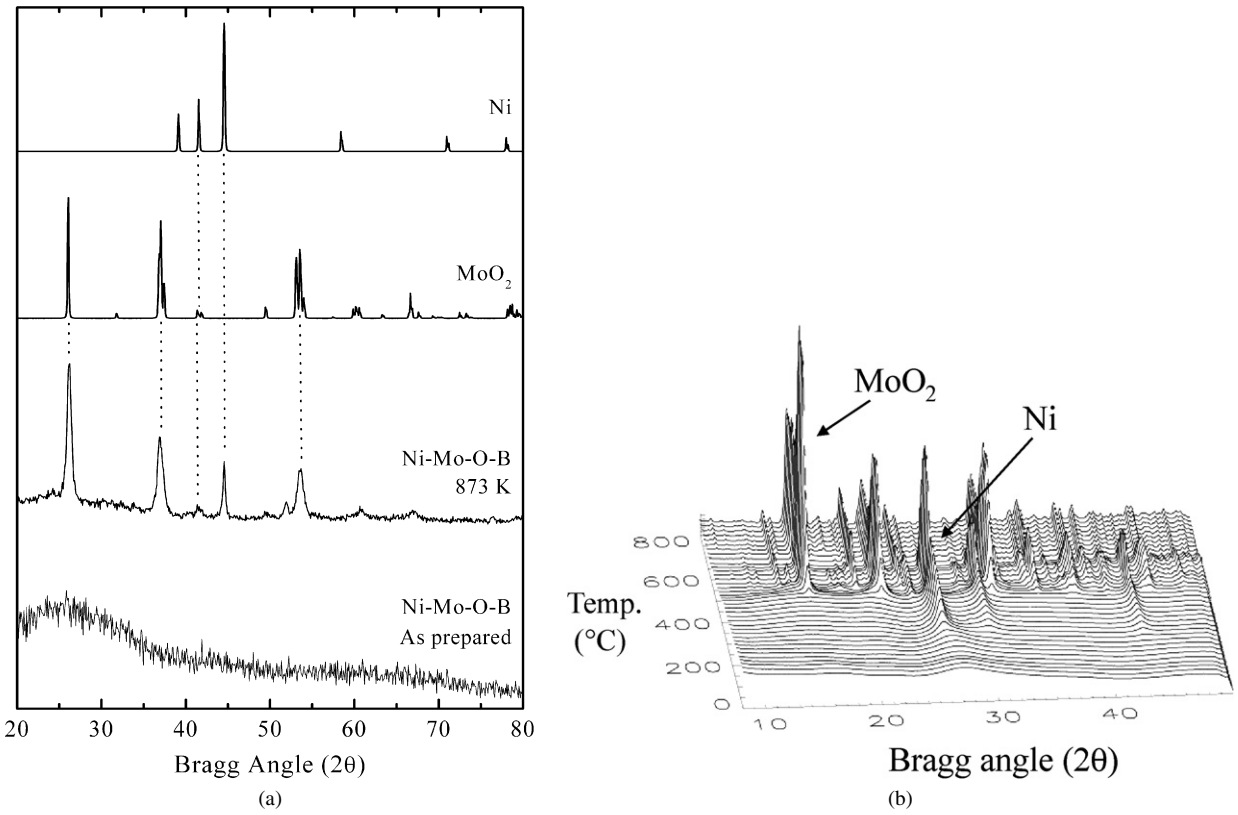

Fig. 9. (a) Conventional XRD patterns ($\lambda = 1.54178$ Å) of an as-prepared unsupported Ni-Mo-O-B catalyst, a Ni-Mo-O-B catalyst annealed to 873 K in flowing He, and reference patterns for MoO_2 and Ni. (b) Time-resolved XRD patterns ($\lambda = 0.9220$ Å) acquired while heating (6.5 K/min) as-prepared unsupported Ni-Mo-O-B catalyst in flowing He.

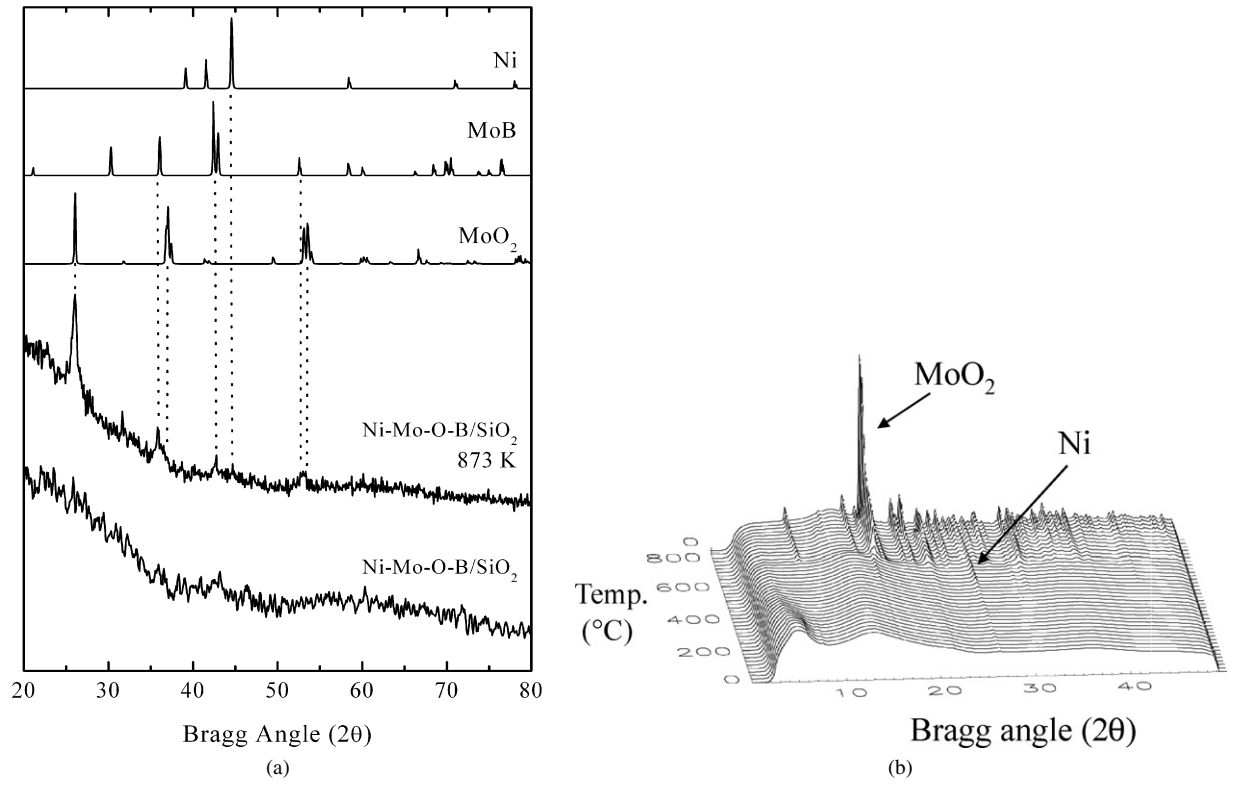

Fig. 10. (a) Conventional XRD patterns ($\lambda = 1.54178$ Å) of an as-prepared Ni-Mo-O-B/SiO_2 catalyst, a Ni-Mo-O-B/SiO_2 catalyst annealed to 873 K in flowing He, and reference patterns for MoO_2 and Ni. (b) Time-resolved XRD patterns ($\lambda = 0.9220$ Å) acquired while heating (6.5 K/min) an as-prepared Ni-Mo-O-B/SiO_2 catalyst in flowing He.

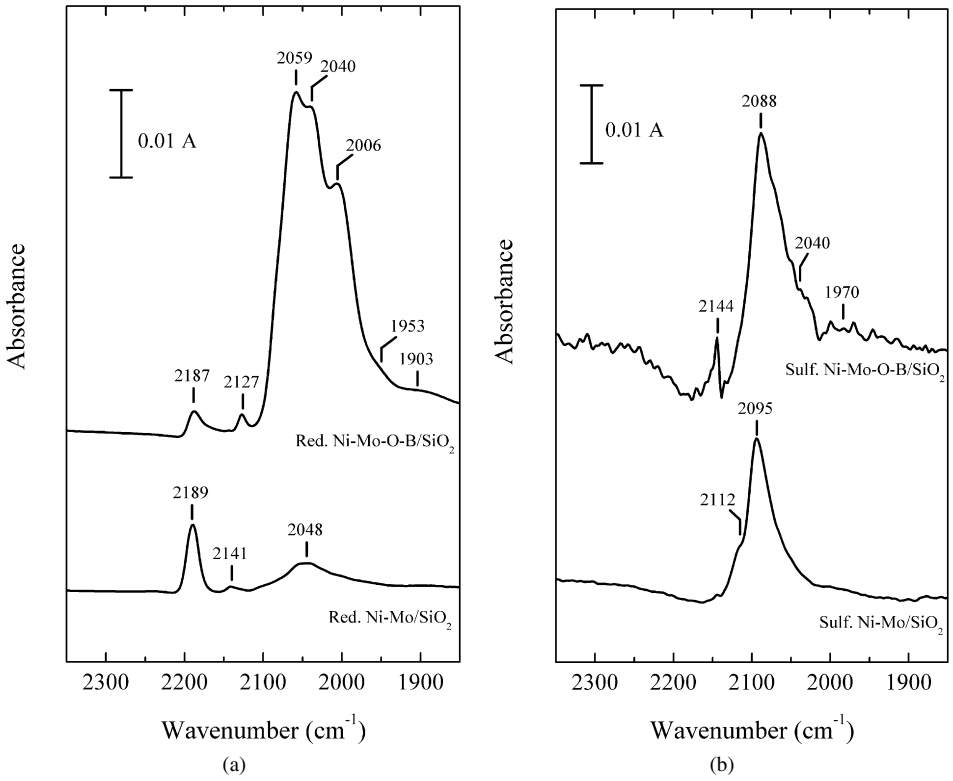

Fig. 11. IR spectra of adsorbed CO on (a) reduced and (b) sulfided Ni-Mo-O-B/SiO_2 and Ni-Mo/SiO_2 catalysts.

bonded CO on Ni^0 sites [45,46], indicating the presence of some unsulfided Ni species on the catalyst surface. Finally, the ν_{CO} absorbances at 2088 and 2144 cm^{-1} are assigned to CO adsorbed on Ni-promoted $Mo^{\delta+}$ and Ni^+ sites, respectively, as described above for Ni-Mo/SiO_2.

3.2. HDS activity

The thiophene HDS activity versus time for reduced and sulfided Ni-Mo-O-B/SiO_2 catalysts and of a sulfided Ni-Mo/SiO_2 catalyst are shown in Fig. 12. The reduced Ni-Mo-O-B/SiO_2 catalyst exhibited a steady HDS activity over the entire 24 h on stream, but its activity after 24 h was lower than that of either the sulfided Ni-Mo/SiO_2 or Ni-Mo-O-B/SiO_2 catalysts. These latter two catalysts both exhibited decreasing HDS activity over time, but the activity of the sulfided Ni-Mo/SiO_2 catalyst decreased more rapidly such that its activity was just 70% of that of the sulfided Ni-Mo-O-B/SiO_2 catalyst after 24 h on stream.

The thiophene HDS activities of the Ni-B/SiO_2, Mo-O-B/SiO_2, and Ni-Mo-O-B/SiO_2 catalysts are plotted in Fig. 13 as a function of the Ni mole fraction (excluding B content) of the catalysts. The HDS activities are for the amorphous metal boron catalysts subjected to a sulfidation pretreatment (see Section 2). XRD patterns of sulfided Ni-B/SiO_2, Mo-O-B/SiO_2, and Ni-Mo-O-B/SiO_2 (Ni/Mo = 0.99) catalysts are shown in Fig. 14. The XRD patterns exhibit a rapidly dropping background similar to those of the as-prepared catalysts, but the patterns for the sulfided Ni-B/SiO_2 and Ni-Mo-O-B/SiO_2 catalysts show additional features. The XRD pattern of the sulfided Ni-B/SiO_2 catalyst shows peaks at 21.5° and 31.3° that can be assigned

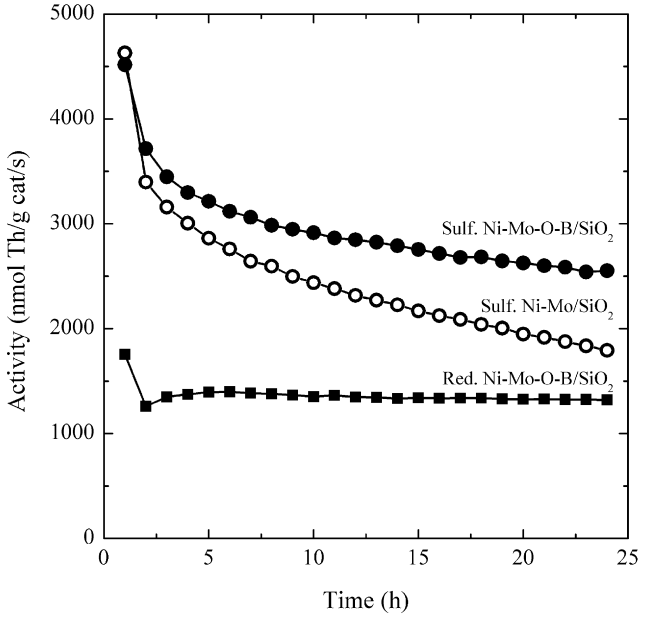

Fig. 12. Thiophene HDS activities of reduced and sulfided Ni-Mo-O-B/SiO_2 catalysts (Ni/Mo = 0.99) and a sulfided Ni-Mo/SiO_2 catalyst (Ni/Mo = 0.50) as a function of the time on-stream.

to Ni_9S_8 (card no. 22-1193), and the pattern for the sulfided Ni-Mo-O-B/SiO_2 catalyst also exhibits a peak at 21.5°.

HDS activities of sulfided Ni/SiO_2, Mo/SiO_2, and Ni-Mo/SiO_2 catalysts prepared by conventional preparation methods are also plotted in Fig. 13. The trend of HDS activities for the conventionally prepared Ni-Mo/SiO_2 catalysts is consistent with those reported previously [7]. A broad maximum

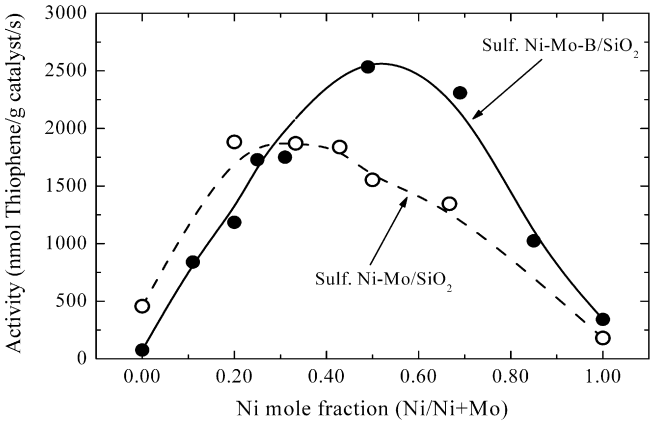

Fig. 13. Thiophene HDS activities of sulfided Ni-Mo-O-B/SiO_2, and Ni-Mo/SiO_2 catalysts as a function of the Ni mole fraction.

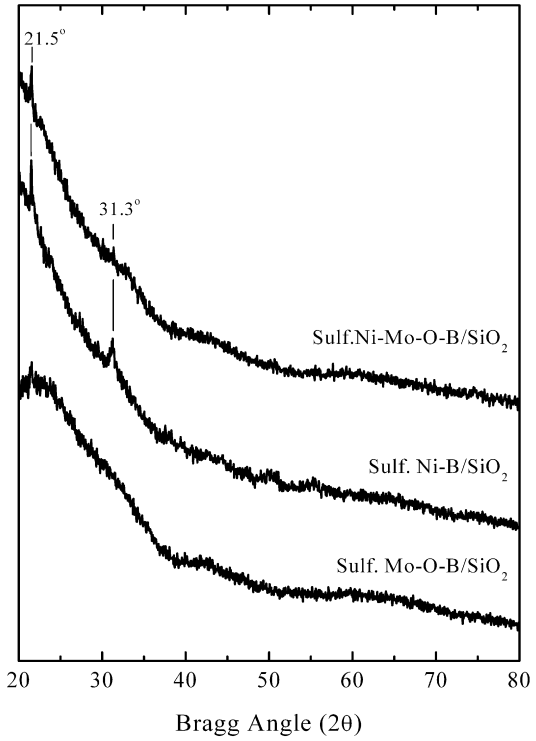

Fig. 14. X-ray diffraction patterns of sulfided Ni-B/SiO_2, Mo-O-B/SiO_2, and Ni-Mo-O-B/SiO_2 catalysts.

in activity is observed for catalysts with molar ratios of Ni/Mo ∼0.5, with an enhancement of activity of approximately four measured relative to an unpromoted sulfided Mo/SiO_2 catalyst. For the sulfided Ni-Mo-O-B/SiO_2 catalysts, the maximum in HDS activity is shifted to a catalyst with a molar ratio of Ni/Mo = 0.99 and corresponds to an activity enhancement of a factor of ∼33 relative to a sulfided Mo-O-B/SiO_2 catalyst, which had a quite low HDS activity. The sulfided Mo-O-B/SiO_2 catalyst (28.7 wt% MoO_3 equivalent, 22 μmol O_2/g) was six times less active than the sulfided Mo/SiO_2 catalyst (30.4 wt% MoO_3, 18 μmol O_2/g), despite having a slightly higher O_2 chemisorption capacity. On the other hand, the sulfided Ni-B/SiO_2 catalyst (27.4 wt% NiO equivalent, 251 μmol O_2/g) was twice as active as the sulfided Ni/SiO_2 catalyst (30.1 wt% NiO, 72 μmol O_2/g), while having an O_2 chemisorption capacity 3.5 times higher than that of the sulfided Ni/SiO_2 catalyst. Comparing the Ni-Mo catalysts, the most active sulfided Ni-Mo-O-B/SiO_2 catalyst (Ni/Mo = 0.99, 9.5 wt% NiO and 18.4 wt% MoO_3 equivalents, 26 μmol O_2/g) was 1.4 times more active than the sulfided Ni-Mo/SiO_2 catalyst with the optimal Ni loading (Ni/Mo = 0.5, 7.9 wt% NiO, 30.4 wt% MoO_3, 23 μmol O_2/g).

4. Discussion

As part of a larger research effort to explore the HDS properties of nonsulfide materials, the focus of this study was catalysts derived from amorphous metal-boron materials. Unsupported and silica-supported Ni-B and Ni-Mo-O-B materials were observed to have substantial B content (B/Me = 0.2–0.5, Me = Ni+Mo), whereas unsupported and silica-supported Mo-O-B had minimal B contents (B/Mo = 0.08–0.1). As summarized in Fig. 13, the Ni-B/SiO_2 and Ni-Mo-O-B/SiO_2 catalysts were more active than their sulfide counterparts (Ni/SiO_2 and Ni-Mo/SiO_2), whereas the Mo-O-B/SiO_2 catalyst was substantially less active than a sulfided Mo/SiO_2 catalyst. Interestingly, the HDS activity versus time data plotted in Fig. 12 indicates that Ni-Mo-O-B/SiO_2 catalysts have distinct HDS properties relative to conventional sulfided Ni-Mo/SiO_2 catalysts. Typical of the activity trends observed for sulfided Mo and Ni-Mo catalysts tested in our laboratory [16,18], the HDS activity of a sulfided Ni-Mo/SiO_2 catalyst (Ni/Mo = 0.5) decreases steadily over the 24-h test period. On the other hand, the reduced Ni-Mo-O-B/SiO_2 catalyst shows a steady HDS activity, whereas the sulfided Ni-Mo-O-B/SiO_2 catalyst exhibits a slowly decreasing activity that appears to be nearing steady-state HDS activity after 24 h. As discussed later, insight into the HDS properties of the catalysts derived from the amorphous Ni-Mo-O-B/SiO_2 materials can be gained from the characterization studies carried out in this work.

Unsupported and supported Ni-B materials have received the greatest attention of amorphous metal-boron materials as catalysts and, as a result, more is understood about the properties of these materials. DSC has been used to indirectly probe the crystallization of unsupported Ni-B and Ni-B on a range of supports. For unsupported Ni-B, DSC reveals a very strong exothermic peak centered at ∼615 K [27]. Li et al. also acquired XRD patterns (independent of the DSC measurements) after annealing Ni-B to increasing temperatures. No changes in the XRD patterns were observed below 573 K, whereas above this temperature crystallization occurred to give predominantly Ni_3B (and a small amount of Ni_2B) at 673–773 K and then metallic Ni above 773 K. The intense DSC peak at ∼615 K, which extends over the temperature range of 500–800 K, corresponds to the crystallization of Ni-B to give Ni_3B and its subsequent decomposition to give Ni metal. This is generally consistent with our conventional XRD results (Fig. 5a), in which we observed a pattern nearly identical to that of a reference pattern for Ni_3B after annealing to 773 K, as well as our time-resolved XRD results (Fig. 5b) that show rapid crystallization of Ni-B starting at ∼633 K. Crystallization of the Ni-B yields Ni_3B, for

which XRD peaks are at a maximum at ∼723 K, followed by formation of Ni metal starting at ∼713 K. The time-resolved XRD measurements provide greater detail concerning the extent of crystallization and the identity of the phases formed than is possible with DSC and conventional XRD.

Despite having a higher B/Ni molar ratio than the unsupported Ni-B, there is no evidence in the conventional and time-resolved XRD patterns for the Ni-B/SiO_2 catalyst for the formation of crystalline B-containing phases. Crystalline Ni is formed starting at ∼533 K, which subsequently converts to NiO starting at ∼813 K, presumably forming via reaction of Ni with OH groups on the support surface and/or surface O in the passivation layer formed on the catalyst surface after synthesis. Interestingly, XRD patterns acquired for a Ni-B/C catalyst indicate a higher crystallization temperature (>600 K) for Ni-B particles on the carbon support, than on either SiO_2 or γ-Al_2O_3 [33,38,44]. In all cases, the only crystalline phase observed to form on the different supports is metallic Ni. Li et al. [38] observed a shift of the exothermic peak in their DSC traces for Ni-B/Al_2O_3 catalysts to lower temperatures with increased Ni loading (11–15 wt% NiO equivalent). Given the high loading of our Ni-B/SiO_2 catalyst (27.4 wt% NiO equivalent), it is not surprising that we observe the first indication of crystallization at the lower temperature of ∼533 K using time-resolved XRD. The XPS peak assigned to reduced Ni species (i.e., not in the passive oxide layer) in the Ni-B/SiO_2 catalyst has a Ni($2p_{3/2}$) binding energy (851.5 eV) below that of Ni metal (853.0 eV). As has been suggested before, B associated with Ni likely donates electron density to Ni atoms in the silica-supported Ni-B. Thus, although no crystalline B-containing phases are observed on annealing our Ni-B/SiO_2 catalyst, the substantial B content in the amorphous Ni-B particles significantly modifies the properties of the Ni. The Ni-B/SiO_2 catalyst, when presulfided, had a thiophene HDS activity nearly twice that of a sulfided Ni/SiO_2 catalyst after 24 h on stream. This observation is not surprising given that the sulfided Ni-B/SiO_2 catalyst had an O_2 chemisorption capacity 3.5 times higher than that of the sulfided Ni/SiO_2 catalyst. TEM images of an as-prepared Ni-B/SiO_2 catalyst (e.g., Fig. 1b) reveal relatively large amorphous Ni-B particles on the support (20–40 nm), so the high chemisorption capacity of this catalyst appears unrelated to a high dispersion of the Ni-B phase. Apparently, the high B content of this catalyst (B/Ni = 0.61) facilitates a high site density on the sulfided Ni-B/SiO_2 catalyst (relative to the sulfided Ni/SiO_2 catalyst) despite the relatively large particle size. An XRD pattern of a sulfided Ni-B/SiO_2 catalyst (Fig. 14) indicates the formation of some Ni_9S_8 in the catalyst as a result of a sulfidation pretreatment at 650 K. Either this Ni sulfide phase formed on the Ni-B particles is highly dispersed or a significant number of adsorption sites exist on unsulfided or partially sulfided portions of the supported Ni-B particles. Suslick et al. [6] observed unsupported Ni_3B to become partially converted to Ni_9S_8 after thiophene HDS for 20 h at the high temperature of 723 K and fully converted to Ni_9S_8 after sulfidation in a 10 mol% H_2S/H_2 mixture at 723 K for 12 h. The HDS activity of the unsupported Ni_3B steadily increased over 15 h on stream, which the authors concluded was due to its conversion to the more catalytically active Ni_9S_8 phase. Due to the high reaction temperature of 723 K, which is above typical HDS processing temperatures (573–673 K) [7], directly comparing the results of Suslick et al. with those of the current study is difficult. At 643 K, we observe that the sulfided Ni-B/SiO_2 catalyst has twice the steady-state HDS activity as a B-free sulfided Ni/SiO_2 catalyst, despite evidence of some bulk Ni_9S_8 formation during presulfidation of the Ni-B/SiO_2 catalyst.

In contrast to the Ni-B/SiO_2 catalyst, the Mo-O-B/SiO_2 catalyst had an HDS activity six times lower than a sulfided Mo/SiO_2 catalyst with a similar Mo loading. This observation is surprising, given that the Mo-O-B/SiO_2 catalyst has a somewhat higher O_2 chemisorption capacity and a very low B content (B/Mo = 0.10) that makes up just 0.22 wt% of the catalyst. The conventional and time-resolved XRD patterns indicate that both unsupported and silica-supported Mo-O-B crystallize to give predominantly MoO_2, with some MoO_3 also present. For the Mo-O-B/SiO_2 catalyst, time-resolved XRD revealed rapid onset of MoO_2 crystallization at ∼623 K, below the sulfidation temperature of 650 K. Thus, it is likely that crystalline MoO_2 on the silica support is the Mo phase that undergoes sulfidation for the Mo-O-B/SiO_2 catalyst. Thomazeau et al. [56] compared sulfided Mo/SiO_2 catalysts prepared from silica-supported MoO_2 and MoO_3 precursors and measured similar thiophene HDS activities. The addition of small amounts of B (<1 wt%) in the form of H_3BO_3 to γ-Al_2O_3 before the preparation of sulfided Co-Mo/Al_2O_3 and Ni-Mo/Al_2O_3 catalysts has been observed to increase HDS activity [8–10]. On the other hand, adding B (as H_3BO_3) after the metals to Co-Mo/Al_2O_3 catalysts produced only a decrease in HDS activity [11]. For the Mo-O-B/SiO_2 catalyst, TEM revealed a large particle size (60–80 nm), but the O_2 chemisorption capacity of the catalyst in sulfided form is somewhat higher than that for the sulfided Mo/SiO_2 catalyst, indicating that the dramatically lower HDS activity is not due to dispersion effects. The XRD pattern of the sulfided Mo-O-B/SiO_2 catalyst shows no evidence of crystalline phases, indicating either that the Mo-containing phase remains amorphous or that the crystallite size is below the detection limit of XRD. Based on the foregoing discussion, no explanation is apparent for the dramatically lower HDS activity of the sulfided Mo-O-B/SiO_2 catalyst, which has a low B content incorporated during $NaBH_4$ (partial) reduction of a $(NH_4)_6Mo_7O_{24}/SiO_2$ precursor, relative to a B-free sulfided Mo/SiO_2 catalyst.

The most important observation of this study is that Ni-Mo-O-B/SiO_2 catalysts with Ni/Mo > ∼0.5, prepared by $NaBH_4$ reduction of metal salt precursors, have higher thiophene HDS activities than conventionally prepared Ni-Mo/SiO_2 catalysts. For example, a Ni-Mo-O-B/SiO_2 catalyst with Ni/Mo = 0.99, when presulfided, had an HDS activity 1.4 times higher than a sulfided Ni-Mo/SiO_2 catalyst with the optimal molar ratio of Ni/Mo = 0.5. These observations are somewhat surprising given that the unpromoted Mo-O-B/SiO_2 catalyst is six times less active than a conventionally prepared sulfided Mo/SiO_2 catalyst, and both amorphous materials crystallize to give the predominant Mo-containing phase of MoO_2. However, the onset of MoO_2 crystallization is shifted >150 degrees higher (to

~790 K) for the Ni-Mo-O-B/SiO_2 catalyst. Similarly, the crystallization of Ni shifts approximately 150 degrees to higher temperature (~675 K) for the Ni-Mo-O-B/SiO_2 catalyst compared with a Ni-B/SiO_2 catalyst. These results (as well as those for the unsupported materials) indicate that the simultaneous reduction of Ni and Mo salts to give a Ni-Mo-O-B phase on the silica support yields an amorphous material that is substantially more resistant to crystallization than when the metal salts are reduced alone. It is important to note, however, that whereas the unsupported and silica-supported Ni-Mo-O-B materials are apparently homogeneous in the as-prepared form, they do still phase-segregate on heating in flowing He to give principally Ni metal and MoO_2, the phases formed from heating the monometallic amorphous metal-boron phases. High-resolution TEM images are consistent with the as-prepared unsupported and silica-supported Ni-Mo-O-B materials being homogeneous as they reveal particles of uniform morphology. The Ni in the Ni-Mo-O-B/SiO_2 catalyst (Ni/Mo = 0.99) is apparently quite well dispersed as the conventional and time-resolved XRD patterns exhibit only very weak peaks associated with Ni metal (and no evidence for Ni-B crystalline phases). The higher dispersion of Ni in the Ni-Mo-O-B/SiO_2 catalysts than in the Ni-Mo/SiO_2 catalysts is further supported by the IR spectral results for adsorbed CO on the catalysts. For the sulfided catalysts (Fig. 11b), the absorbance feature assigned to Ni-promoted $Mo^{\delta+}$ sites is substantially larger for the Ni-Mo-O-B/SiO_2 catalyst than for the Ni-Mo/SiO_2 catalyst, and the spectrum of the latter also shows an absorbance feature associated with unpromoted Mo^{2+} sites that is not apparent in the spectrum of the sulfided amorphous metal-boron catalyst. Although directly comparing the IR spectra for the reduced catalysts (Fig. 11a) is more difficult, because some of the Ni in the Ni-Mo-O-B/SiO_2 catalyst is already reduced in the as-prepared catalysts before the H_2 treatment (as indicated by XPS), the dramatically larger absorbance features in the ν_{CO} region associated with CO linearly bonded to Ni^0 for the Ni-Mo-O-B/SiO_2 catalyst also point to a higher Ni dispersion for this catalyst relative to the Ni-Mo/SiO_2 catalyst. Therefore, we conclude that the use of $NaBH_4$ to reduce the Ni and Mo salts yields Ni-Mo-O-B/SiO_2 catalysts with very highly dispersed Ni species. This likely explains why the optimal Ni/Mo molar ratio of 0.99 for the Ni-Mo-O-B/SiO_2 catalysts is twice that of the conventionally prepared Ni-Mo/SiO_2 catalyst, for which the optimal Ni/Mo molar ratio is 0.50, because more Ni that effectively promotes Mo can be accommodated in catalysts prepared via $NaBH_4$-based synthesis. It follows that the Ni-Mo-O-B/SiO_2 catalyst with the optimal Ni/Mo molar ratios is significantly more active for thiophene HDS compared with the conventionally prepared Ni-Mo/SiO_2 catalyst with its optimal Ni/Mo molar ratio. An XRD pattern of a sulfided Ni-Mo-O-B/SiO_2 catalyst (Ni/Mo = 0.99) reveals a small peak at 21.5° suggesting that a small amount of Ni has been converted to Ni_9S_8, a phase with low HDS activity. Previous studies of alumina-supported Co_3Mo_3N and Ni_3Mo_3N materials sulfided under similar conditions showed substantially stronger XRD peaks for Co_9S_8 in the former and MoS_2 in both catalysts [13,57]. By comparison, the amorphous Ni-Mo-O-B/SiO_2 catalyst is less susceptible to the formation of crystalline sulfide phases as a result of sulfidation pretreatment. This resistance, along with the high Ni dispersion, contributes to the high HDS activity of the Ni-Mo-O-B/SiO_2 catalysts.

What remains unclear is the chemical environment of B in the Ni-Mo-O-B/SiO_2 catalysts. The Ni-B and Ni-Mo-O-B materials have similar boron-to-metal molar ratios (B/Me ~0.5) and similar XPS spectra in the Ni(2p) and B(1s) regions. However, whereas unsupported Ni-B crystallizes to give Ni_3B starting at 633 K, unsupported Ni-Mo-O-B begins to crystallize at 550 K to give Ni metal, and no crystalline B-containing phases are formed at higher temperatures. Apparently, B is less strongly associated with Ni in Ni-Mo-O-B than in Ni-B, resulting in crystallization of the Ni at a lower temperature. For the silica-supported phases, the greatest difference between Ni-B and Ni-Mo-O-B is that very little crystalline Ni is formed in the Ni-Mo-O-B/SiO_2 on annealing, whereas a substantial Ni peak forms for the Ni-B/SiO_2, again reinforcing the conclusion that Ni is highly dispersed in the former catalyst. Finally, although no definitive conclusions can be drawn about the chemical environment of B in the catalysts, given the significant O content of the unsupported and silica-supported Ni-Mo-O-B (relative to the Ni-B materials) and the foregoing discussion, it seems likely that at least some of the B is bonded primarily to O in a form that does not yield a crystalline phase on annealing in flowing He.

5. Conclusion

Sulfided Ni-B/SiO_2 and Ni-Mo-O-B/SiO_2 catalysts, in which the precursors were prepared by $NaBH_4$ reduction of silica-supported metal salts, had significantly higher thiophene HDS activities than conventionally prepared sulfided Ni/SiO_2 and Ni-Mo/SiO_2 catalysts. On the other hand, a sulfided Mo-O-B/SiO_2 catalyst had dramatically lower HDS activity than a sulfided Mo/SiO_2 catalyst. Based on the results of various physicochemical characterization measurements, including time-resolved XRD, the high HDS activities of sulfided Ni-B/SiO_2 and Ni-Mo-O-B/SiO_2 catalysts are traced to a high density of active sites on these materials compared with conventionally prepared catalysts.

Acknowledgments

This research was supported by the National Science Foundation under grant CHE-0101690 and the Camille and Henry Dreyfus Scholar/Fellow Program for Undergraduate Institutions. Some of the research described in this paper (TEM, XPS) was performed in the Environmental Molecular Sciences Laboratory (EMSL), a national scientific user facility sponsored by the Department of Energy's Office of Biological and Environmental Research and located at Pacific Northwest National Laboratory. The research carried out at the NSLS beam line X7b was supported under contract DE-AC02-98CH10886 with the U.S. Department of Energy, Office of Basic Energy Sciences, Chemical Science Division. The NSLS is supported by the Divisions of Materials and Chemical Sciences of the U.S. Department of Energy.

References

[1] H.I. Schlessinger, H.C. Brown, A.E. Finholt, J.R. Gilbreath, J. Am. Chem. Soc. 75 (1953) 215.
[2] R.C. Wade, Catal. Rev. Sci. Eng. 14 (1976) 211.
[3] J.-F. Deng, H. Li, W. Wang, Catal. Today 51 (1999) 113.
[4] C. Luo, W.-N. Wang, M.-H. Qiao, K.-N. Fan, J. Mol. Catal. A 184 (2002) 379.
[5] Q.-Y. Cheng, W. Li, J. Wu, N.-J. Guan, K.-Y. Tao, Ran Liao Hua Xue Xue Bao 28 (2000) 249.
[6] S. Skrabalak, K. Suslick, Chem. Mater. 18 (2006) 3103.
[7] H. Topsøe, B. Clausen, F.E. Massoth, in: J.R. Anderson, M. Boudart (Eds.), Catalysis: Science and Technology, vol. 11, Springer-Verlag, Berlin, 1996, p. 1.
[8] J. Ramirez, P. Castillo, L. Cedeno, R. Cuevas, M. Castillo, J.M. Palacios, A. Lopez-Agudo, Appl. Catal. A 132 (1995) 317.
[9] D. Li, T. Sato, M. Imamura, H. Shimada, A. Nishijima, J. Catal. 170 (1997) 357.
[10] Usman, T. Kubota, Y. Araki, K. Ishida, Y. Okamoto, J. Catal. 227 (2004) 523.
[11] G. Muralidhar, F.E. Massoth, J. Shabtai, J. Catal. 85 (1984) 44.
[12] T. Kabe, A. Ishihara, W. Qian, Hydrodesulfurization and Hydrodenitrogenation: Chemistry and Engineering, Wiley–VCH, Weinheim, 1999.
[13] B. Diaz, S.J. Sawhill, D.H. Bale, R. Main, D.C. Phillips, S. Korlann, R. Self, M.E. Bussell, Catal. Today 86 (2003) 191.
[14] D.C. Phillips, S.J. Sawhill, R. Self, M.E. Bussell, J. Catal. 207 (2002) 266.
[15] J.A. Rodriguez, J.-Y. Kim, J.C. Hanson, S.J. Sawhill, M.E. Bussell, J. Phys. Chem. B 107 (2003) 6276.
[16] S.J. Sawhill, D.C. Phillips, M.E. Bussell, J. Catal. 215 (2003) 208.
[17] S.J. Sawhill, K.A. Layman, D.R. Van Wyk, M.H. Engelhard, C. Wang, M.E. Bussell, J. Catal. 231 (2005) 300.
[18] P.A. Aegerter, W.W.C. Quigley, G.J. Simpson, D.D. Ziegler, J.W. Logan, K.R. McCrea, S. Glazier, M.E. Bussell, J. Catal. 164 (1996) 109.
[19] K.R. McCrea, J.W. Logan, T.L. Tarbuck, J.L. Heiser, M.E. Bussell, J. Catal. 171 (1997) 255.
[20] G.N. Glavee, K.J. Klabunde, C.M. Sorenson, Langmuir 10 (1994) 4726.
[21] P. Norby, J.C. Hanson, Catal. Today 39 (1998) 301.
[22] P.J. Chupas, M.F. Ciraolo, J.C. Hanson, C.P. Grey, J. Am. Chem. Soc. 123 (2001) 1694.
[23] X. Wang, J.C. Hanson, G. Liu, J.A. Rodriguez, A. Iglesias-Juez, M. Fernandez-Garcia, J. Chem. Phys. 121 (2004) 5434.
[24] A.P. Hammersley, S.O. Svensson, A. Thompson, Nucl. Instrum. Methods Phys. Res. A 346 (1994) 312.
[25] Research Systems, Inc., Boulder, CO, 2002.
[26] A.L. Diaz, M.E. Bussell, J. Phys. Chem. 97 (1993) 470.
[27] H. Li, Y. Wu, Y. Wan, J. Zhang, W. Dai, M. Qiao, Catal. Today 93–95 (2004) 493.
[28] Y.-Z. Chen, B.-J. Liaw, S.-J. Chiang, Appl. Catal. A 284 (2005) 97.
[29] J. Fang, X. Chen, S. Yan, M. Qiao, H. Li, H. He, K. Fan, J. Catal. 229 (2005) 97.
[30] S.-T. Wong, J.-F. Lee, J.-M. Chen, C.-Y. Mou, J. Mol. Catal. A 165 (2001) 159.
[31] H. Li, H. Li, W.-L. Dai, J.-F. Deng, Appl. Catal. A 207 (2001) 151.
[32] R. Paul, P. Buisson, N. Joseph, Ind. Eng. Chem. 44 (1952) 1006.
[33] H. Li, H. Li, J.-F. Deng, Catal. Today 74 (2002) 53.
[34] P. Dufresne, E. Payen, J. Grimblot, J.P. Bonnelle, J. Phys. Chem. 85 (1981) 2344.
[35] D. Briggs, M.P. Seah (Eds.), Practical Surface Analysis by Auger and X-ray Photoelectron Spectroscopy, Wiley, New York, 1983.
[36] Y. Okamoto, Y. Nitta, T. Imanaka, S. Teranishi, J. Chem. Soc. Faraday Trans. 75 (1980) 2027.
[37] J.A. Schreifels, P.C. Maybury, W.E. Swartz, J. Catal. 65 (1980) 195.
[38] J. Li, M. Qiao, J.-F. Deng, J. Mol. Catal. A 169 (2001) 295.
[39] C.D. Wagner, A.V. Naumkin, A. Kraut-Vass, J.W. Allison, C.J. Powell, J.R. Rumble Jr., NIST X-ray Photoelectron Spectroscopy Database, version 3.4, vol. 2005, National Institute of Standards and Technology, 2003.
[40] Y. Okamoto, K. Fukino, T. Imanaka, S. Teranishi, J. Catal. 74 (1982) 173.
[41] H. Belatel, H. Al-Kandari, F. Al-Khorafi, A. Katrib, F. Garin, Appl. Catal. A 275 (2004) 141.
[42] JCPDS Powder Diffraction File, International Centre for Diffraction Data, Swarthmore, PA, 2000.
[43] Z. Jiang, H. Yang, Z. Wei, Z. Xie, W. Zhong, S. Wei, Appl. Catal. A 279 (2005) 165.
[44] Y. He, M. Qiao, H. Hu, J.-F. Deng, K. Fan, Appl. Catal. A 228 (2002) 29.
[45] C.H. Rochester, R.J. Terrel, J. Chem. Soc. Faraday Trans. 73 (1977) 609.
[46] D.G. Blackmond, E.I. Ko, J. Catal. 96 (1985) 210.
[47] J.B. Peri, J. Phys. Chem. 86 (1982) 1615.
[48] J.L.G. Fierro, A. Lopez Agudo, L.G. Tejuca, J. Chem. Soc. Faraday Trans. 81 (1985) 1203.
[49] A.A. Davydov, Infrared Spectroscopy of Adsorbed Species on the Surface of Transition Metal Oxides, Wiley, New York, 1990.
[50] E.C. DeCanio, J.C. Edwards, T.R. Scalzo, D.A. Storm, J.W. Bruno, J. Catal. 132 (1991) 498.
[51] E.C. DeCanio, D.A. Storm, J. Catal. 132 (1991) 375.
[52] M. Angulo, F. Mauge, J.C. Duchet, J.C. LaValley, Bull. Soc. Chim. Belg. 96 (1987) 925.
[53] F. Maugé, J.C. Lavalley, J. Catal. 137 (1992) 69.
[54] B. Müller, A.D. van Langeveld, J.A. Moulijn, H. Knözinger, J. Phys. Chem. 97 (1993) 9028.
[55] B.M. Vogelaar, P. Steiner, A.D. van Langeveld, S. Eijsbouts, J.A. Moulijn, Appl. Catal. A 251 (2003) 85.
[56] C. Thomazeau, V. Martin, P. Afanasiev, Appl. Catal. A 199 (2000) 61.
[57] J.W. Logan, J.L. Heiser, K.R. McCrea, B.D. Gates, M.E. Bussell, Catal. Lett. 56 (1998) 165.